COLD-FORMED STEEL RESEARCH CONSORTIUM

Seismic Behavior of Steel BRBF Buildings Including Consideration of Diaphragm Inelasticity

Gengrui Wei, Matthew R. Eatherton, Hamid Foroughi, Shahab Torabian, Benjamin W. Schafer

March 2020

COLD-FORMED STEEL RESEARCH CONSORTIUM
REPORT SERIES
CFSRC R-2020-04

SDII
Steel Diaphragm Innovation Initiative

About the authors

G. Wei is a Ph.D. candidate at Virginia Tech working with advisor M.R. Eatherton, Associate Professor at Virginia Tech. PhD candidate H. Foroughi, Associate Research Scientist S. Torabian, and Professor B.W. Schafer of Johns Hopkins University also contributed to this study.

CFSRC Information

The Cold-Formed Steel Research Consortium (CFSRC) is a multi-institute consortium of university researchers dedicated to providing world-leading research that enables structural engineers and manufacturers to realize the full potential of structures utilizing cold-formed steel. More information can be found at www.cfsrc.org. All CFSRC reports are hosted permanently by the Johns Hopkins University library in the DSpace collection: https://jscholarship.library.jhu.edu/handle/1774.2/40427.

SDII Information

The Steel Diaphragm Innovation Initiative (SDII) is a multi-year industry-academic partnership to advance the seismic performance of steel floor and roof diaphragms utilized in steel buildings through better understanding of diaphragm-structure interaction, new design approaches, and new three-dimensional modeling tools that provided enhanced capabilities to designers utilizing steel diaphragms in their building systems. SDII was created through collaboration between the American Iron and Steel Institute and the American Institute of Steel Construction with contributions from the Steel Deck Institute, the Metal Building Manufacturers Association, and the Steel Joist Institute in partnership with the Cold-Formed Steel Research Consortium; including, researchers from Johns Hopkins University, Virginia Tech, Northeastern University, and Walter P Moore.

Acknowledgements

This work was supported by the National Science Foundation under Grant No. 1562669 and the Steel Diaphragm Innovation Initiative which is funded by AISC, AISI, SDI, SJI, and MBMA. The Advanced Research Computing (ARC) at Virginia Tech provided high-performance computing resources which facilitated the computational study. Any opinions expressed in this paper are those of the authors alone, and do not necessarily reflect the views of the National Science Foundation.

ABSTRACT

Compared to vertical elements of a building's seismic force resisting systems, our understanding of the horizontal elements, i.e. the diaphragms, is grossly lacking. Recent research showed that diaphragm design forces that have been in the building codes for decades are not sufficiently large to protect the diaphragm from inelastic actions. That research led to the development of the alternative diaphragm design provisions in ASCE 7-16 which use larger diaphragm force demands, but also allows reduction by a diaphragm response modification factor, R_s, that accounts for diaphragm ductility.

In this study, the effect of different diaphragm designs on the behavior of steel buildings is investigated using three-dimensional computational building models that consider nonlinear behavior in both the vertical and horizontal elements of the seismic force resisting system. Three different diaphragm design scenarios are investigated: 1) a conventional design using typical diaphragm design procedures from Section 12.10.1 of ASCE 7-16, 2) an alternative design based on Section 12.10.3 of ASCE 7-16 with R_s = 1.0, and 3) an alternative design with R_s = 2 for composite deck diaphragm and R_s = 2.5 for bare deck diaphragm. A series of 1, 4, 8, and 12-story archetype buildings with 100 ft x 300 ft plan area and perimeter lateral force resisting system consisting of buckling restrained braced frames (BRBF) were designed to the current U.S. building code. The computational models are three-dimensional assemblies of frame elements and truss elements that are capable of capturing yielding of the buckling restrained braces, plastic hinging of the beams and columns, nonlinear behavior of the diaphragm and geometric nonlinearity (i.e., second order effects). The nonlinear behavior of the diaphragm is captured using truss elements with calibrated hysteretic behavior to match past test data from cantilever diaphragm tests. Using these nonlinear computational models of the archetype buildings, modal analyses were conducted to study their modal properties, nonlinear pushover analyses to investigate their static behavior, and nonlinear response history analyses to evaluate their seismic performance including probability of collapse.

Results of the eigenvalue analyses showed that the consideration of diaphragm flexibility led to an increase in first mode period between 13% and 48%. A comparison of results from pushover

analyses and response history analyses indicated that even though the pushover analyses (based on a first mode load pattern) identified the BRBF as being weaker than the diaphragms and therefore dominating the inelastic pushover behavior, response history analyses demonstrated that the diaphragms can experience substantial inelasticity during a dynamic response. The response history results also suggest that there would be a significant difference in seismic behavior of buildings modeled as two-dimensional (2D) planar frames as compared to the three-dimensional (3D) structures modeled herein. For instance, the median of the peak story drift was approximately 1.5 to 2 times larger than the median of the peak story drift in each of the two orthogonal directions. Furthermore, the observed final collapse mode involves an interaction between large BRBF story drifts combined with diaphragm deformations that are additive and exacerbate second order effects leading to collapse.

The percentage of 44 sets of ground motions that are predicted to cause collapse across all buildings and diaphragm designs is 3.5%, 16.4%, and 32.6% for the design earthquake (DE), maximum considered earthquake (MCE), and an earthquake scale level from FEMA P695 associated with an adjusted collapse margin ratio where 50% collapse is allowable ($ACMR_{10\%}$), respectively. A comparison with results of similar studies in the literature using 2D frames shows that the current 3D models experience more collapses, likely due to consideration of 3D behavior with deformable diaphragms and bidirectional ground motions which results in larger story drifts and larger second-order effects. Although the number of collapses at the DE and MCE hazard levels is larger than desirable, it is expected that these collapses are primarily associated with 3D effects other than diaphragm design. This is further supported by observing that the change in median story drifts was negligible when the R_s value was changed from 2.0 for composite deck diaphragm and R_s = 2.5 for bare deck diaphragm to 1.0. For the $ACMR_{10\%}$ hazard level, the number of collapses is acceptable per FEMA P695 for the 1-story through the 8-story buildings (less than 50%), but exceeds the limit for the 12-story buildings (58.1% for R_s=2 or 2.5 and 54.5% for R_s = 1.0). However, it is observed that the collapse of the 12-story buildings is associated with the BRBFs, not the diaphragm, and the number of collapses is only reduced by 3.6% if the diaphragm is designed using R_s = 1.0 as compared to the larger values. Therefore, it is concluded that the alternative diaphragm design procedure with proposed R_s values listed above (R_s = 2 for

composite deck diaphragm and R_s = 2.5 for bare deck diaphragm) did not have a significant adverse effect on seismic performance of the considered BRBF buildings compared to R_s = 1.0, and thus these R_s values may be reasonable for use in design of these types of structures. Further research is required to understand the behavior of 3D models that consider diaphragm deformations as compared to the more widely used 2D frame analyses, and to define more refined performance objectives (e.g. collapse ratios).

TABLE OF CONTENTS

LIST OF TABLES

LIST OF FIGURES

1. Introduction

Steel building systems with braced frames, steel deck roof diaphragms, and composite concrete on steel deck floor diaphragms are one of the most common structural systems in North America. During an earthquake, lateral inertial forces are transferred through the diaphragms to the vertical portions of the lateral force resisting system (LFRS). Conventional seismic design of these steel buildings assumes that the vertical elements of the LFRS control the dynamics of the building and that they are also the primary source of inelastic actions and hysteretic energy dissipation in the structure. However, it has been shown that diaphragms designed using traditional design procedures may be subject to inelasticity during design level earthquakes (Rodriguez et al, 2007), and in the extreme may cause collapse such as happened for several concrete parking garages with precast concrete diaphragms during the 1994 Northridge earthquake (EERI, 1996).

Current U.S. seismic design provisions ASCE 7-16 (ASCE, 2016) provide two methodologies for seismic design of diaphragms: traditional diaphragm design procedures using forces reduced by the response modification factor, R, associated with the vertical system, and alternative diaphragm design procedures using larger and more accurate elastic design forces. The alternative diaphragm design procedures incorporate a diaphragm design force reduction factor, R_S, that reduces the diaphragm demands based on the ductility and overstrength in the diaphragm. However, currently there is no R_S factor available for steel deck or concrete on steel deck diaphragms, although values for R_S have been proposed for inclusion in the upcoming edition of NERHRP Recommended Seismic Provisions including R_S = 2.5 for steel deck diaphragms satisfying specific special detailing requirements and R_S = 2.0 for composite concrete on steel deck diaphragms.

To explore the impact of different diaphragm design procedures on the seismic performance of building systems, a computational study using three-dimensional (3D) building models that capture nonlinear diaphragm behavior and its interaction with the nonlinear vertical LFRS was conducted. This report presents details of the study starting with definition of a series of 1, 4, 8,

and 12-story archetype buildings with buckling-restrained braced frames (BRBF) for the vertical system and three designs for the diaphragms. The modeling scheme uses computationally efficient calibrated frame and truss elements to capture the realistic nonlinear behavior of both the BRBFs and the diaphragms. Modal analysis, nonlinear static pushover analyses, and nonlinear response history analyses using 44 ground motion records scaled to three hazard levels were performed to investigate the behavior and seismic performance of the buildings.

The objectives of this study include: 1) to examine the effect of diaphragms on the dynamic properties of buildings, 2) to understand the extents of diaphragm inelasticity at specified diaphragm hazard levels, 3) to investigate the probability of collapse for buildings designed using different diaphragm design approaches, and 4) to evaluate whether the use of proposed values of R_S for steel deck and concrete on steel deck diaphragms has a significant effect on the seismic behavior of buildings.

2. Development of Archetype Buildings

A series of 1, 4, 8, and 12-story steel buildings with BRBFs for the vertical LFRS were selected as archetype buildings for this study and designed to the current US building code (Torabian et al, 2019). Three different diaphragm design scenarios were considered: 1) Traditional Design using conventional diaphragm design procedures from Section 12.10.1 of ASCE 7-16 (ASCE, 2016), 2) Alternative 1 using the alternative diaphragm design procedures from Section 12.10.3 of ASCE 7-16 with R_s = 1.0, and 3) Alternative 2 using the alternative diaphragm design procedures with R_s = 2.0 for composite concrete on steel deck diaphragm and R_s = 2.5 for bare steel deck diaphragm.

For 1-story buildings, two different types of roof system were considered, i.e., a composite concrete on steel deck roof, and a bare steel deck roof. The 1-story buildings with composite concrete on steel deck roof may be less common than those with bare steel deck roof, but they were included to enable comparison to multi-story buildings with composite concrete on steel deck floors. For all other multi-story buildings, bare steel deck roof and composite concrete on steel deck floors were used. Table 1 shows a list of the buildings analyzed in this study. Note that the diaphragm force demands in the traditional design and the alternative design with R_s = 2.0 for composite floors and R_s =2.5 for the bare steel deck roof (Alternative 2) are controlled by the minimum value allowed for diaphragm design forces (see Table 4 for details), and therefore the archetype buildings designed with these two diaphragm design procedures were identical.

Table 1 List of BRB Archetype Buildings for the Study

Building Number	Number of Stories	Diaphragm Design
1	1	Traditional / Alternative 2 (R_s = 2.5 with bare steel deck roof)
2	1	Alternative 1 (R_s = 1 with bare steel deck roof)
3	1	Traditional / Alternative 2 (R_s = 2.0 with composite concrete on steel deck roof)
4	1	Alternative 1 (R_s = 1 with composite concrete on steel deck roof)
5	4	Traditional / Alternative 2 (R_s = 2 for floors, R_s =2.5 for roof)
6	4	Alternative 1 (R_s = 1 for floors and roof)
7	8	Traditional / Alternative 2 (R_s = 2 for floors, R_s =2.5 for roof)
8	8	Alternative 1 (R_s = 1 for floors and roof)
9	12	Traditional / Alternative 2 (R_s = 2 for floors, R_s =2.5 for roof)
10	12	Alternative 1 (R_s = 1 for floors and roof)

Table 2 provides the loading information used in the design of the archetype buildings and associated typical seismic weights. Detailed site information and design parameters are given in Table 3, including the location, risk category, importance factor I_e, spectral response acceleration parameter at short periods S_s, spectral response acceleration parameter at a period of 1 sec S_1, site class, response modification coefficient R, overstrength factor Ω_0, deflection amplification factor C_d, approximate fundamental period of the building T_a, upper limit on approximate fundamental period $C_u T_a$, fundamental period of the building obtained from a SAP2000 model T_{model}, effective seismic weight of the building W, and design base shear V.

Table 2 Archetype Building Loading and Design Information

Composite Concrete on Steel Deck Floor / Roof	Bare Steel Deck Roof	Seismic Weight	Site Information	Design Parameters
Dead Load = 56.5 psf slab + 22 psf superimposed = 78.5 psf Live Load = 50 psf + 15 psf partition = 65 psf Exterior wall = 40 psf	Dead Load = 3 psf slab + 22 psf superimposed = 25 psf Live Load = 20 psf + 15 psf partition = 35 psf Exterior wall = 40 psf	Typical Floor = 2545 kips Composite Concrete on Steel Deck Roof = 2630 kips Bare Steel Deck Roof = 1271 kips	Irvine, CA Risk Category 2 I_e = 1.0 S_s = 1.55 S_1 = 0.57 Site Class D	R = 8 Ω_0 = 2.5 C_d = 5

Table 3 Prototype Building Seismic Design Information

Design Parameter	1-story Bare Deck Roof	1-story Composite Roof	4-story	8-story	12-story
T_a (sec)	0.96	0.11	0.58	0.96	1.30
$C_u T_a$ (sec)	0.30	0.30	0.81	1.34	1.81
T_{model} (sec)	0.46	0.41	0.76	1.31	2.00
W (kip)	1271	2630	8906	19086	29266
V (kip)	164	339	830	1036	1326

The buildings all use the same plan dimensions, shown in Figures 1 and 2, 300 ft by 100 ft with a story height of 14 ft at the first story and 12.5 ft for a typical story. Four bays of BRBFs are located on the perimeter of the building in each orthogonal direction and Figure 3 shows an elevation view of the BRBFs in the 4-story building. Typical details for the floor and roof diaphragms are given in notes on Figures 1 and 2, as designed based on the diaphragm design forces tabulated in Table 4. Members sizes for each archetype building are provided in Tables A-1, A-2, and A-3 in the Appendix. Additional details for the design of the archetype buildings can be found in Torabian et al (2019).

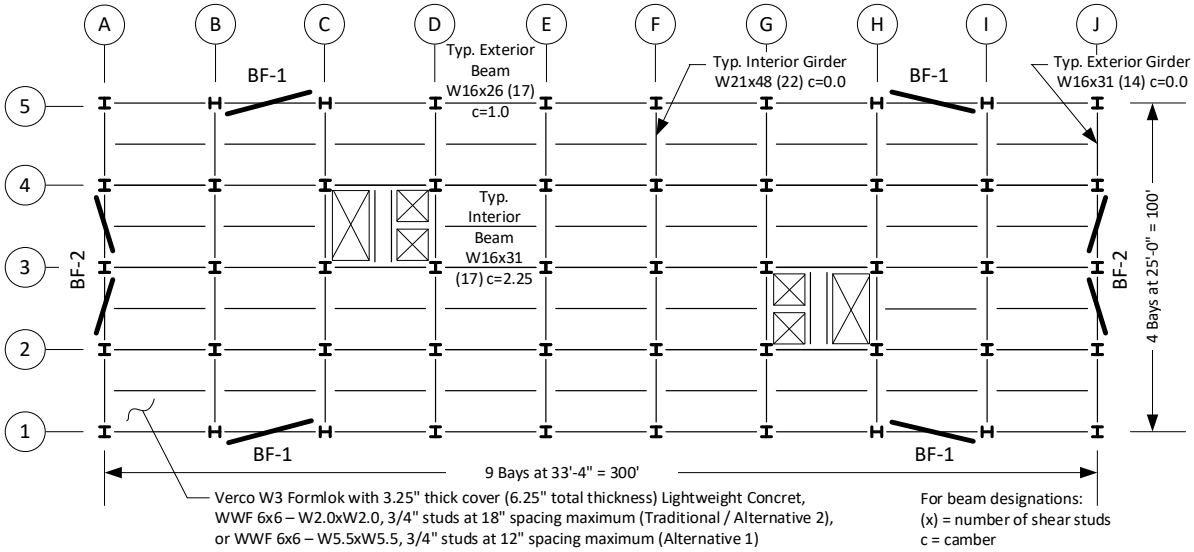

Figure 1 Typical Floor Framing Plan

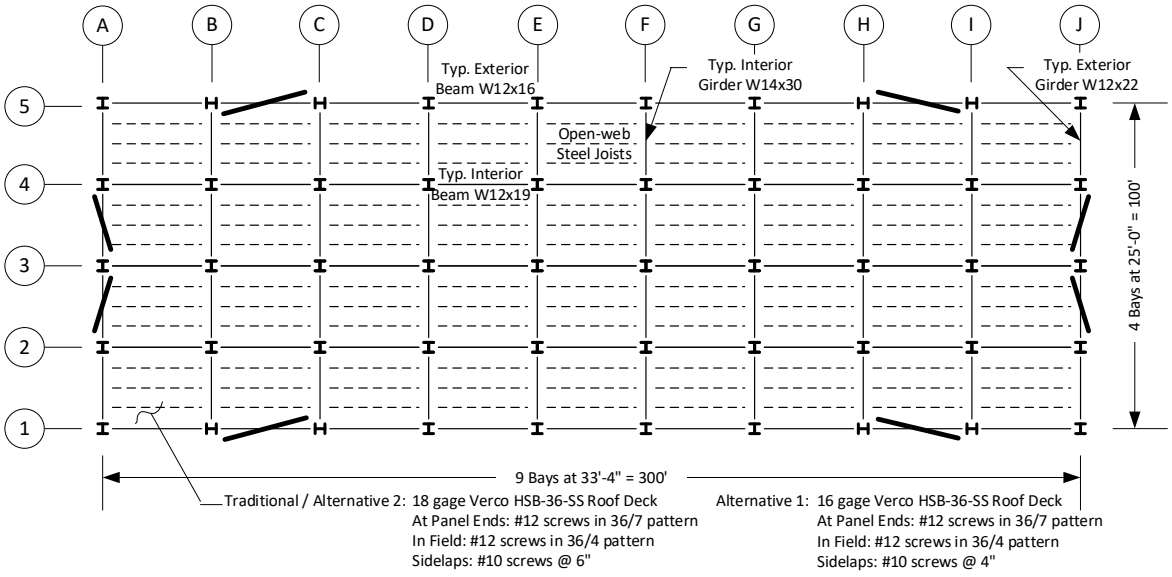

Figure 2 Typical Roof Framing Plan

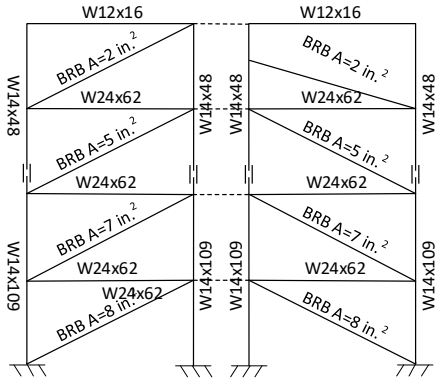

(a) BRB frame on gridlines 1 and 5

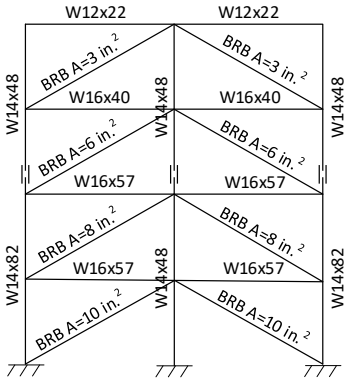

(b) BRB frame on gridlines A and J

Figure 3 Elevation view of 4-story building braced frames

Table 4 Diaphragm Design Shear per Unit width at Diaphragm Edge along Short Dimension of Building

Archetype Building	Level	Diaphragm Design Forces (kip/ft)		
		Traditional*	Alternative 1	Alternative 2*
1-story (bare steel deck roof)	Roof	1.31	2.10	1.31
1-story (composite concrete on steel deck roof)	Roof	2.71	4.27	2.71
4-story	Roof	1.31	2.10	1.31
	2-4	2.62	4.25	2.62
	3	2.62	4.57	2.62
	2	2.62	4.89	2.62
8-story	Roof	1.31	2.10	1.31
	8	2.62	4.19	2.62
	7	2.62	4.25	2.62
	6	2.62	4.42	2.62
	5	2.62	4.58	2.62
	4	2.62	4.74	2.62
	3	2.62	4.90	2.62
	2	2.62	5.06	2.62
12-story	Roof	1.31	2.10	1.31
	12	2.62	4.19	2.62
	11	2.62	4.19	2.62
	10	2.62	4.26	2.62
	9	2.62	4.36	2.62
	8	2.62	4.47	2.62
	7	2.62	4.58	2.62
	6	2.62	4.69	2.62
	5	2.62	4.80	2.62
	4	2.62	4.91	2.62
	3	2.62	5.01	2.62
	2	2.62	5.12	2.62

*: All diaphragm design forces for the Traditional and Alternative 2 design were controlled by the minimum, $0.2S_{DS}$ multiplied by the diaphragm seismic weight.

3. Development of Computational Models

Nonlinear 3D computational models were created using the *OpenSees* software (Mazzoni et al, 2006), a structural analysis program widely used for earthquake engineering simulations. Figure 4 shows a schematic view of the 1, 4, 8, and 12-story archetype building models used in this study. Details of the modeling shceme is provided in this section.

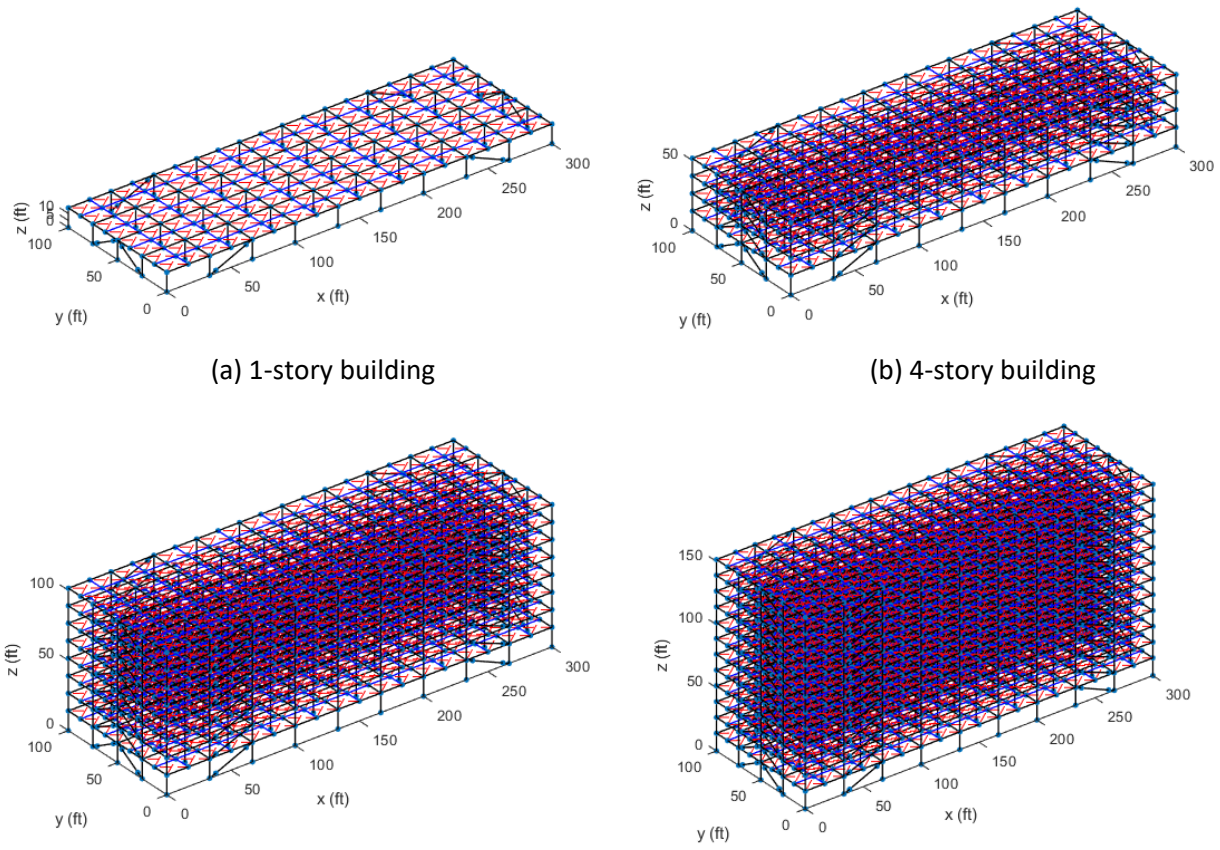

(a) 1-story building

(b) 4-story building

(c) 8-story building

(d) 12-story building

Figure 4 3D OpenSees models of archetype buildings

3.1. Modeling of Diaphragms

Truss elements were used to simulate the in-plane diaphragm behavior in the archetype buildings. The load-deformation behavior of a diaphragm is typically obtained through cantilever diaphragm tests in which a steel deck diaphragm with or without concrete fill is supported with one edge fixed and the parallel edge subjected to a shear loading (Figure 5a). Using the force-

displacement data from these types of tests, computational models with diagonal nonlinear truss elements of unit cross-section area (Figure 5b) were calibrated to capture the behavior of the diaphragm tests. All connections were modeled as pinned, and the perimeter framing beams were modeled as nonlinear beam-column elements with kinematic hardening material and with the same size of cross sections as the test. Figure 6 shows the meshing of diaphragms in the computational models of the archetype buildings. The dimension of the diaphragm unit in the mesh is 200 in.×150 in., which is similar in scale to the test specimens used for calibration.

The cantilever diaphragm test database established by O'Brien et al (2017) was utilized as a tool to help select specimens for diaphragm model calibration. For the roof diaphragm, the specimen labeled as Test 33 by Martin (2002) with 20-gage P3615 1.5 in. B-deck was selected to satisfy the force demand for the archetype building roof diaphragm with Traditional / Alternative 2 design procedures (herein denoted as SP1). For the floor diaphragm, test specimen 3/6.25-4-L-NF-DT tested by Avellaneda Ramirez et al (2019) was used, which consisted of 3 in. deck, with lightweight concrete fill and 6.25 in. total thickness (herein denoted as SP2). The dimensions of the test specimens (240 in.×144 in. for SP1 and 180 in.×144 in. for SP2) are close to those of the diaphragm units in the mesh of the building models.

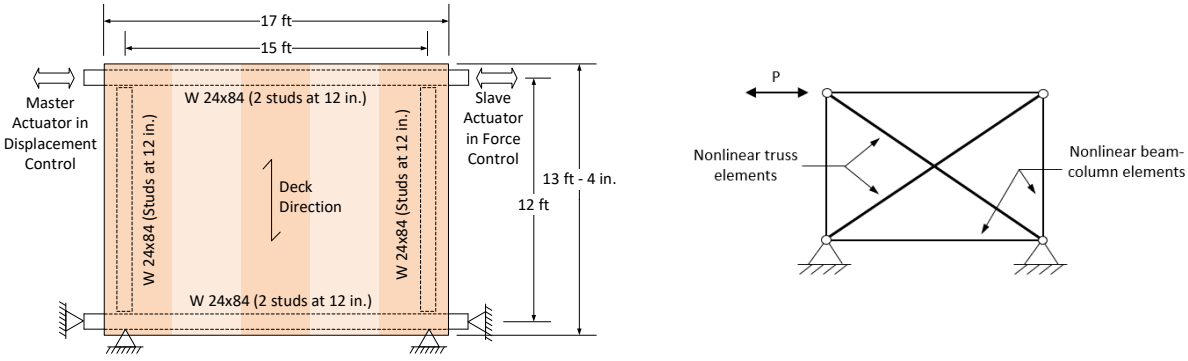

(a) Schematic view of SP2 test setup (b) Computational model

Figure 5 Test setup and computational model of cantilever diaphragm test

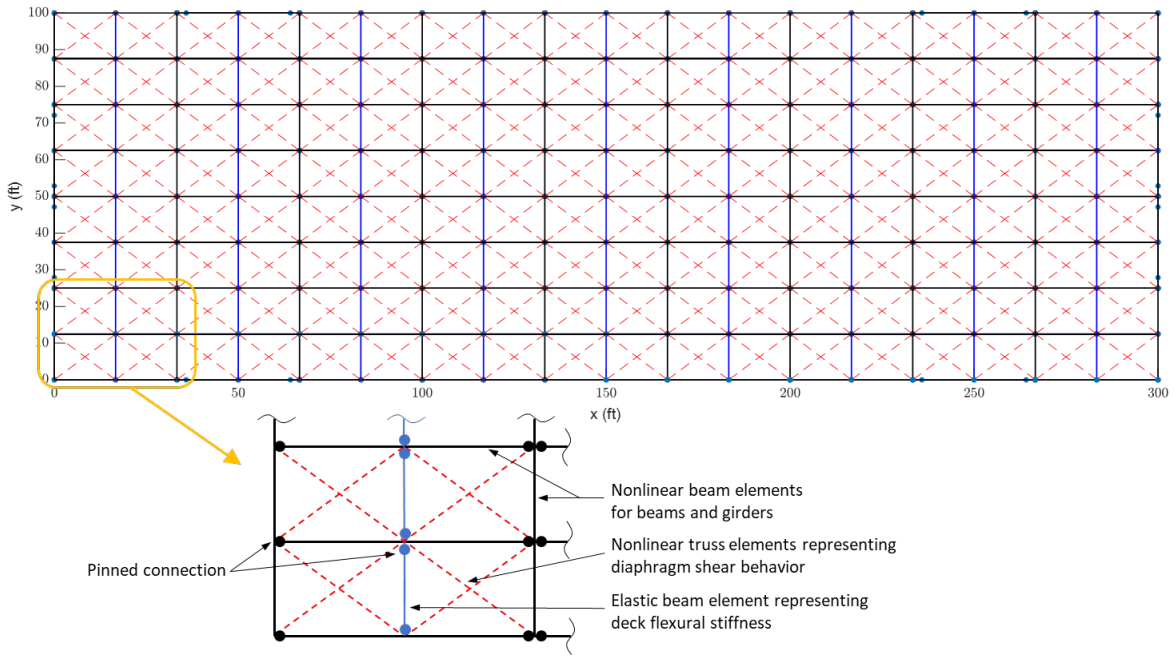

Figure 6 Diaphragm meshing in computational models of archetype buildings

As is shown in Figure 7, the Pinching4 material model in OpenSees was used for the truss elements. This model is capable of capturing the hysteretic pinching, cyclic strength degradation, and cyclic stiffness degradation behavior of diaphragms. Material parameters for the Pinching4 model, including backbone stresses and strains and cyclic strength and stiffness degradation parameters, were calibrated through a six-step optimization algorithm to achieve an optimal match between hysteretic response from the simulation and test that minimizes the objective functions:

1) The experimental stress-strain backbone curve was first obtained from the cyclic test data, and was simplified to a curve with multiple linear segments as defined by Pinching4 model, where the third characteristic point was obtained at the peak load of the backbone, and the first, second, and fourth points were obtained by interpolation at 40%, 80%, and 40% (for SP1) or 30% (for SP2), respectively, of the peak load on the backbone. The initial stress-strain backbone was obtained by scaling the backbone of the cyclic cantilever test data with a factor equal to 1.3, which was selected from multiple runs of the optimization algorithm with the different scale factors for the initial stress-strain backbone such that

the sum of the errors for peak forces, reloading stiffness, unloading stiffness, and cumulative energy dissipation of the hysteretic loops, considering different weights for each type of error, was the minimum.

2) The strength degradation parameters considering displacement and energy history are optimized to achieve a minimum error for the peak forces of the hysteretic loops.
3) The reloading stiffness degradation parameters considering displacement and energy history are optimized to achieve a minimum error for the reloading stiffness of the hysteretic loops.
4) The unloading stiffness degradation parameters considering displacement and energy history are optimized to achieve a minimum error for the unloading stiffness of the hysteretic loops.
5) The parameters for reloading / unloading are optimized to achieve a minimum error for the cumulative energy dissipation in the hysteretic loops.
6) All the Pinching4 parameters are optimized together to achieve a minimum value for an objective function defined as the sum of the errors for peak forces, reloading stiffness, unloading stiffness, and cumulative energy dissipation of the hysteretic loops, considering different weights for each type of error.

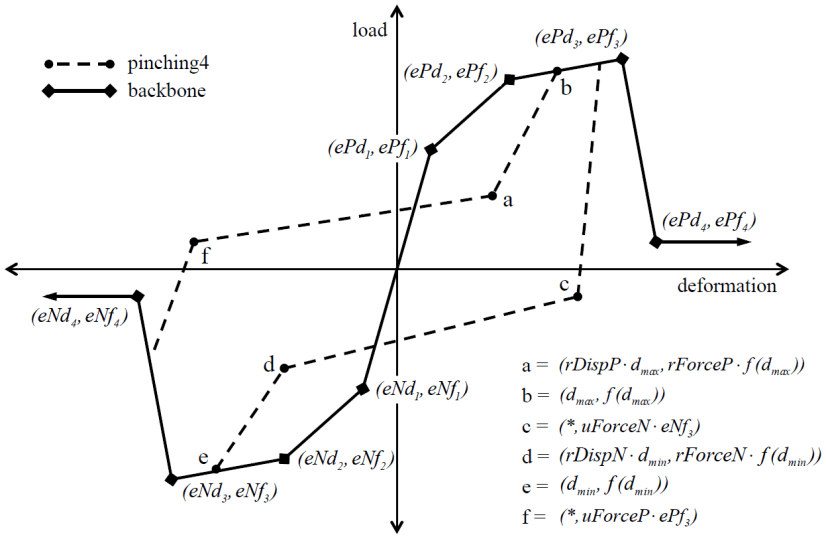

Figure 7 Pinching4 material model

Table 5 shows the resulting values of the Pinching4 material model parameters for the two selected diaphragm specimens. It should be noted that the dimensions of the archetype building diaphragm units do not coincide with those of the test specimens, and therefore the backbone parameters were modified using the strategy described in the Appendix so that the diaphragm shear strength per unit length is consistently represented. A comparison of the hysteretic response from the calibrated diaphragm simulation and that from the experiment is shown in Figure 8.

Table 5 Calibrated Pinching4 Material Model Parameters

Test	Backbone				Pinching			Strength Degradation					Stiffness Degradation					Energy Dissipation
	ε_1, σ_1 (ksi)	ε_2, σ_2 (ksi)	ε_3, σ_3 (ksi)	ε_4, σ_4 (ksi)	r_{Δ^+}, r_{Δ^-}	r_{F^+}, r_{F^-}	u_{F^+}, u_{F^-}	gF_1	gF_2	gF_3	gF_4	gF_{lim}	gK_1, gD_1	gK_2, gD_2	gK_3, gD_3	gK_4, gD_4	gK_{lim}, gD_{lim}	gE
SP1	0.0008, 22.18	0.0017, 28.90	0.0033, 30.69	0.0053, 23.97	0.20, 0.35	0.20, 0.35	0.10, 0.12	0	0.35	0	0.70	0.90	0, 0	0, 0.50	0, 0	0, 0.75	0, 0.90	4.31
SP2	0.0005, 63.46	0.0006, 76.41	0.0014, 107.40	0.0143, 48.33	-0.06, -0.06	0.12, 0.12	0.11, 0.11	0	0.83	0.0	0.46	0.33	1.09, 0.14	0.76, 0.47	0.32, 0.12	0.75, 0.10	1.04, 0.61	4.29

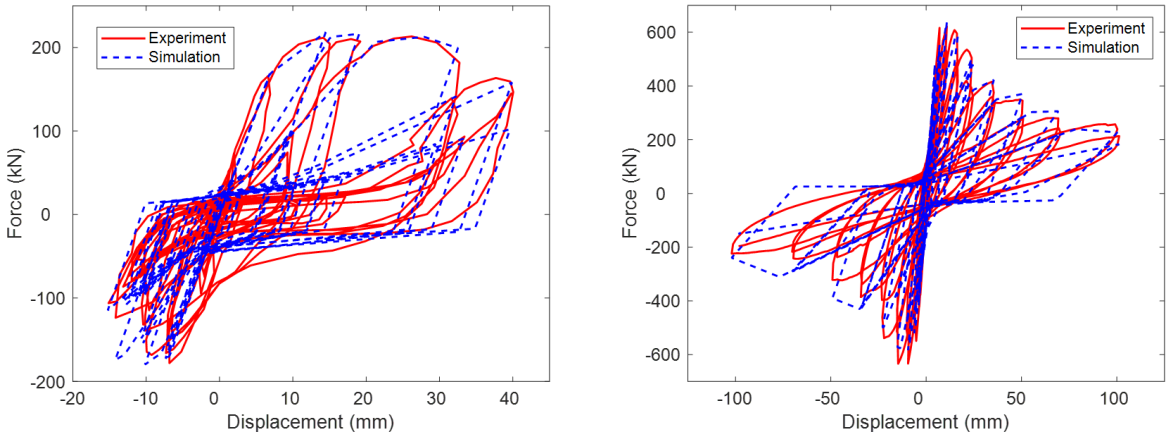

(*a*) SP1 (*b*) SP2

Figure 8 Hysteretic response of diaphragm from experiment and simulation

Table 6 provides the diaphragm demands and designs using ASD for the archetype buildings, where v is the shear demand per unit width of the diaphragm (as given in Table 4 in detail), Ω is the safety factor for ASD ($\Omega = 1.5$), and v_a is the allowable strength of the diaphragm given by the manufacturers based on the resulting design as described in the notes of Table 6. For the

models of the same archetype building with different diaphragm designs that are not a perfect match with past testing, the same Pinching4 model parameters were used except that the backbone stresses were scaled so that the peak strength exactly equals the expected nominal strength of the diaphragm from design. In this case, no overstrength of the diaphragm is considered. The expected nominal strength is calculated with prediction equations to the best knowledge of the authors. For bare steel deck diaphragm, DDM04 (Luttrell et al., 2015) and AISI 310-16 (AISI, 2016) are used to calculate the nominal strength. For concrete on steel deck diaphragm, the nominal strength is determined as the lesser of: the strength associated with concrete slab diagonal tension cracking limit state calculated with the proposed equations (for AISI S310 2022 edition) in O'Brien et al 2017, in addition to the contribution of reinforcing steel which is calculated with ACI 318-14; and the strength associated with the perimeter fastener limit state calculated per AISC 360-16 (AISC, 2016). The expected nominal strength and scale factors are given in Table 7, where v_{pred} is the expected nominal strength of the diaphragm design, and v_{exp} is the peak strength from hysteretic curve.

Table 6 Diaphragm Demands and Design

Archetype Building			v (kip/ft)	v/Ω (kip/ft)	Diaphragm Design	v_a (kip/ft)
1-story (bare steel deck roof)	Traditional / Alternative 2		1.31	0.87	Bare Deck 1*	1.04
	Alternative 1		2.10	1.40	Bare Deck 2*	1.73
1-story (comp. deck roof)	Traditional / Alternative 2		2.67	1.78	Composite 1*	1.81
	Alternative 1		4.27	2.85	Composite 2*	3.70
4-story	Traditional / Alternative 2	Roof	1.31	0.87	Bare Deck 1	1.04
		Levels 1-3	2.62	1.75	Composite 1	1.81
	Alternative 1	Roof	2.10	1.40	Bare Deck 2	1.73
		Levels 1-3	4.25-4.89	3.26	Composite 2	3.70
8-story	Traditional / Alternative 2	Roof	1.31	0.87	Bare Deck 1	1.04
		Levels 1-7	2.62	1.75	Composite 1	1.81
	Alternative 1	Roof	2.10	1.40	Bare Deck 2	1.73
		Levels 1-7	4.19-5.06	3.37	Composite 2	3.70
12-story	Traditional / Alternative 2	Roof	1.31	0.87	Bare Deck 1	1.04
		Levels 1-11	2.62	1.75	Composite 1	1.81
	Alternative 1	Roof	2.10	1.40	Bare Deck 2	1.73
		Levels 1-11	4.19-5.12	3.41	Composite 2	3.70

*: Details of the diaphragm design are given as follows.

Bare Deck 1: 18 gage HSB®-36-SS steel deck, 36/7/4 #12 screw pattern at supports, #10@6" sidelap attachments.
Bare Deck 2: 16 gage HSB®-36-SS steel deck, 36/7/4 #12 screw pattern at supports, #10@4" sidelap attachments.
Composite 1: Verco W3 Formlok with 3.25" thick lightweight concrete cover (6.25" total thickness, f_c' = 3 ksi), WWF 6×6 – W2.0×W2.0, 3/4" studs at 18" spacing maximum
Composite 2: Verco W3 Formlok with 3.25" thick lightweight concrete cover (6.25" total thickness, f_c' = 3 ksi), WWF 6×6 – W5.5×W5.5, 3/4" studs at 12" spacing maximum

Table 7 Diaphragm Nominal Strength and Backbone Stress Scale Factors

Archetype Building			v_{pred} (kip/ft)	Limit State of v_{pred}	v_{exp} (kip/ft)	Limit State of v_{exp}	Scale Factor
1-story (bare steel deck roof)	Trad. / Alt. 2		2.18	connection	2.41	sidelap fastener	0.906
	Alt. 1		3.50	connection	2.41	sidelap fastener	1.452
1-story (comp. deck roof)	Trad. / Alt. 2		11.40	connection	9.55	sidelap fastener	1.194
	Alt. 1		16.79	connection	9.55	sidelap fastener	1.758
4-story	Trad. / Alt. 2	Roof	2.18	connection	2.41	sidelap fastener	0.906
		Levels 1-3	11.40	perim. fastener	9.55	diag. tension crack.	1.194
	Alt. 1	Roof	3.50	connection	2.41	sidelap fastener	1.452
		Levels 1-3	16.79	diag. tension crack.	9.55	diag. tension crack.	1.758
8-story	Trad. / Alt. 2	Roof	2.18	connection	2.41	sidelap fastener	0.906
		Levels 1-7	11.40	perim. fastener	9.55	diag. tension crack.	1.194
	Alt. 1	Roof	3.50	connection	2.41	sidelap fastener	1.452
		Levels 1-7	16.79	diag. tension crack.	9.55	diag. tension crack.	1.758
12-story	Trad. / Alt. 2	Roof	2.18	connection	2.41	sidelap fastener	0.906
		Levels 1-11	11.40	perim. fastener	9.55	diag. tension crack.	1.194
	Alt. 1	Roof	3.50	connection	2.41	sidelap fastener	1.452
		Levels 1-11	16.79	diag. tension crack.	9.55	diag. tension crack.	1.758

The limit states that control the nominal strength calculation and the experimental strength are also provided in Table 7. While it would be ideal to use test specimens that match the predicted limit states, test data was not available for some of the diaphragm configurations and limit states considered herein at the time this study was conducted. Therefore, the test specimens selected were used to represent some of the diaphragm designs even though their limit states do not match exactly. This was deemed acceptable for concrete on steel deck diaphragms whose limit states differ considerable, as it can be shown with other experimental test data (Eatherton et al., 2020) that the hysteretic behavior of a test specimen with the limit state of v_{pred} is similar to that of the specimen selected herein. Also, it can be observed that the allowable strength of the

diaphragms v_a in Table 6 is substantially smaller than the predicted strength v_{pred} given in Table 7, which is due to the ASD safety factor and conservation in current diaphragm design.

3.2. Modeling of Buckling-Restrained Braces

As shown in Figure 9, the BRB core (restrained yielding segment) is represented by a nonlinear truss element with *Steel4* material model in *OpenSees*, the non-yielding segments on both ends are modeled with elastic beam-column elements (with cross-section area equal to 10 times that of the BRB core), and another elastic beam-column element with negligible cross-section area and large bending stiffness is also used to connect the non-yielding segments to fix the rotational degrees of freedom and prevent instability of the truss element.

The material model for the BRB core was calibrated to match the behavior of specimens tested by Newell et al (2006). All specimens from the test (Specimens 1G, 2G, 3G, and 4G) were examined, and the maximum cross-section area of the BRBs in the archetype building is 14 in^2, which is closest to Specimens 1G and 2G (12 in^2). However, Specimen 2G had increased compressive strength during large displacement cycles due to the bearing of core plate against the confining HSS. As a representative option, the calibrated Steel4 material parameters for Specimen 1G were used in the archetype building modeling and the values are given in Table 8. Figure 10 shows the hysteretic curves of the calibrated model as compared to test results from Specimens 1G and 3G. For the building models, the same parameters and configuration of the BRB model were used, except that the cross section area of the core brace was changed to match the BRB design of the buildings. Figure 11 shows a schematic view of BRB modeling in the 4-story archetype building.

The fatigue material model *uniaxialMaterial Fatigue* in *OpenSees* was also calibrated to capture BRB fracture. The only specimen from Newell et al. (2006) that fractured was Specimen 3, and therefore its test data was used in the calibration. Two parameters were calibrated: ε_0, the strain at which one cycle will cause failure, and m, the slope of Coffin-Manson curve (Coffin, 1954; Manson, 1954) in log-log space. The value of ε_0 was assumed to be 0.2 based on an appropriate elongation at fracture of an ASTM A36 plate subjected to monotonic tension test per

ASTM standards (ASTM, 2019). The value of m was set equal to –0.5976 to produce fracture at a point in the simulation close to that in the test of Specimen 3G.

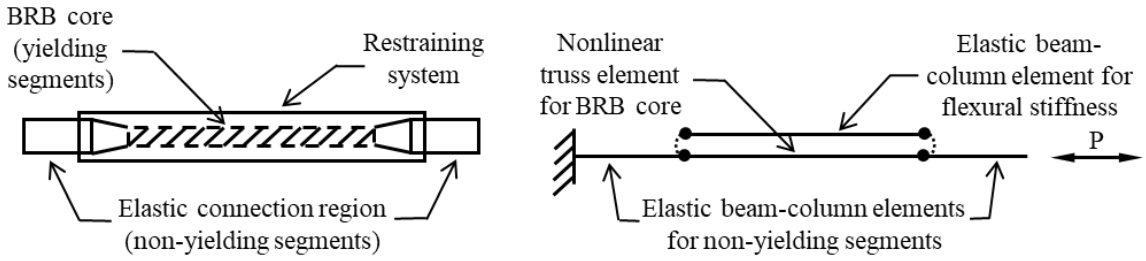

(a) Schematic BRB assembly (b) Computational model

Figure 9 Configuration of a typical BRB and computational model

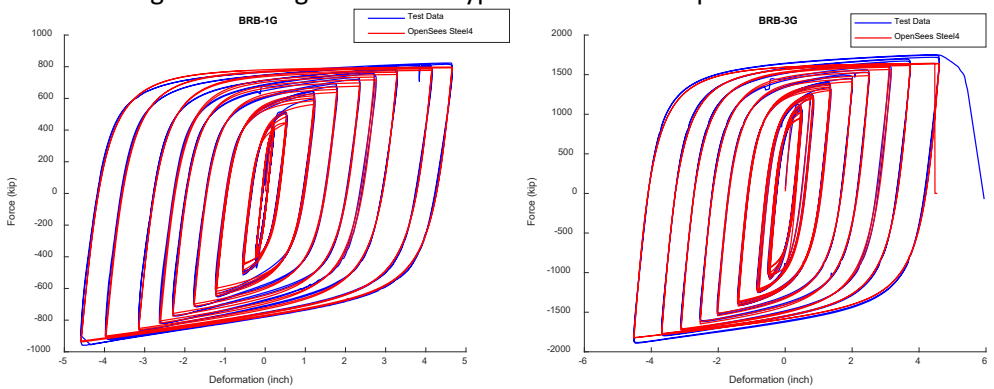

(a) Specimen 1G (b) Specimen 3G

Figure 10 Calibration of BRB Steel4 models for Specimens 1G and 3G

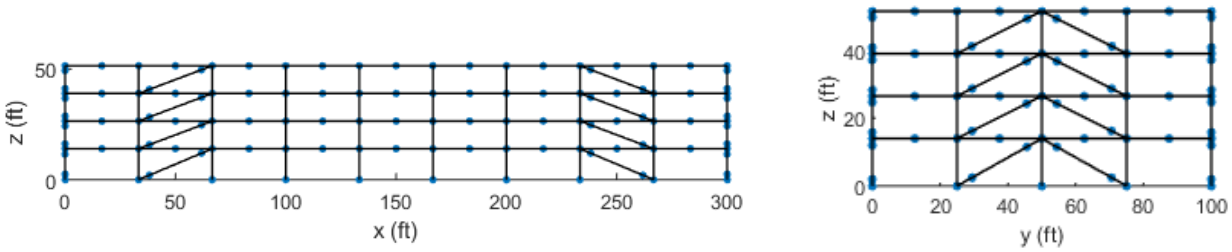

(a) x-z view (b) y-z view

Figure 11 Schematic view of BRB modeling in 4-story archetype building

Table 8 Calibrated Steel4 Parameters

b_k	R_0	r_1	r_2	b_i	b_l	ρ_i	R_i	l_{yp}	f_u	R_u
0	20.9837	0.9122	0.1209	0.0306	0	0.7262	1.3134	18.2022	70.3000	620.6286
b_{kc}	R_{0c}	r_{1c}	r_{2c}	b_{ic}	b_{lc}	ρ_{ic}	R_{ic}	l_{ypc}	f_{uc}	R_{uc}
0.0121	18.9116	0.9133	0.1232	0.0020	0	0.9061	2.9727	37.3548	108.4701	583.5268

3.3. Other Modeling Details

Some additional details of the models are discussed in this section.

3.3.1. Boundary Conditions and Joint Fixity

All columns were pinned at the base and continuous over the building height. All the beam-to-column and beam-to-beam joints were pinned except for the beam-to-column joints of the BRB frames which were made rigid for all degrees of freedom. The reason for making these connections rigid is that in practice these connections have substantial gusset plates, welds and/or bolts that make them effectively act as a moment connection.

3.3.2. Gravity Loads and Masses

As recommended by FEMA P695 (FEMA, 2009) the gravity loads included a combination of dead loads and live loads (1.05D+0.25L). Masses were determined from the dead loads and lumped at the column nodes on each floor. Masses at typical node locations are given in Table 9.

Table 9 Masses at Typical Node Locations

Level	Masses at Different Locations (kip-sec^2/in.)			
	Corner	Left/Right Edge	Top/Bottom Edge	Interior
Roof	0.046	0.059	0.067	0.070
Typical Floor	0.077	0.110	0.121	0.155
2nd Floor	0.079	0.112	0.123	0.155

3.3.3. Material and Geometric Nonlinearity

Both material and geometric nonlinearity were considered in the analysis. In addition to the aforementioned nonlinear material models used for diaphragms and BRB's, the columns and beams were represented by nonlinear beam-column elements with fiber-section formulation and kinematic hardening material with a hardening modulus equal to 450 ksi. Geometric nonlinearity was considered by including the gravity loads and using the P-Delta coordinate transformation algorithm in *OpenSees* for the columns.

3.3.4. Damping

For nonlinear response history analyses, Rayleigh damping with a critical damping ratio equal to 2% for the 1st and 4th modes was used for the archetype building models.

3.3.5. Encouraging Convergence

An algorithm with multiple steps was developed to encourage convergence in the nonlinear response history analyses and is described as follows. Starting from the first trial for convergence at each time step, if convergence fails, then the algorithm will move to the next trial step. A flow chart of the convergence algorithm is also shown in Figure 12.

1) Use a convergence criterion based on the unbalanced energy (*EnergyIncr*) with tolerance equal to 1e-12 kip-in.
2) Try all available algorithms for solving system equations (*Newton*, *ModifiedNewton*, *NewtonLineSearch*, *Broyden*, and *KrylovNewton*).
3) Reduce the applied displacement increment for pushover analysis or the time step for response history analysis by a factor of 10.
4) Reduce the applied displacement increment for pushover analysis or the time step for response history analysis by a factor of 100.
5) Temporarily relax convergence criterion with the tolerance amplified by a factor of 10.
6) Temporarily relax convergence criterion with the tolerance amplified by a factor of 100.
7) Change the convergence criterion to the one based on the norm of unbalanced forces (*NormUnbalance*) with an initial value of tolerance equal to 1e-5 (unit in kip and kip-in.).
8) Go through Steps 2 to 6 again.
9) Change the convergence criterion to the one based on the norm of displacement increment (*NormDispIncr*) with an initial value of tolerance equal to 1e-6 (unit in in. and rad.).
10) Go through Steps 2 to 6 again.
11) For response history analysis, increase the Rayleigh damping ratio of the whole structure to 5% and then 10% to facilitate the convergence of a certain time step.

12) If all these attempts do not work, the simulation is considered to have experienced convergence failure and the analysis is terminated.

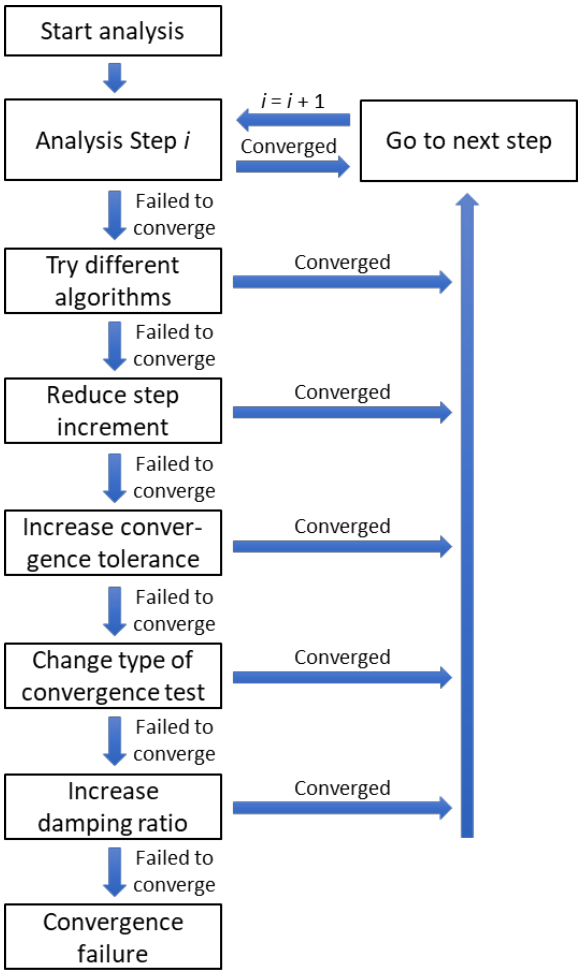

Figure 12 Flow chart of the algorithm for convergence tests

3.4. Processing of Analysis Results

A wide range of structural response quantities were obtained from the analyses, such as nodal displacements, element deformations, element forces, and reactions. These results have been post-processed to calculate other local deformation variables including story drift ratio and diaphragm shear angle (i.e. shear strain), which are described in this section.

3.4.1. Story Drift Ratio Calculation

For pushover analysis, roof drift ratio is defined as the applied displacement at the top of the building divided by the building height. For response history analysis, story drift ratio (SDR) at any time in the record is determined for the x and y directions at each story, which is defined as the x and y relative displacements of any two nodes on the adjacent floors with the same x and y coordinates, divided by the story height. The resultant story drift ratio at any time in the record is calculated by taking the square root of the sum of the squares (SRSS) of the story drift ratios in the x and y directions at that time. The peak story drift ratio is then determined by the largest value of the resultant story drift ratio at any time during the motion and at any location of the building.

3.4.2. Diaphragm Shear Angle Calculation

Diaphragm shear angle (shear strain) is calculated at the center of each diaphragm unit, and is given by the following equation:

$$\gamma = \frac{\partial u_x}{\partial y} + \frac{\partial u_y}{\partial x} \tag{1}$$

where u_x and u_y are the displacement at the center of diaphragm unit along *x* and *y* direction, respectively. u_x and u_y are obtained using piecewise finite element approximation:

$$u_x = \sum_{i=1}^{4} N_i(x,y) u_{x,i} \tag{2}$$

$$u_y = \sum_{i=1}^{4} N_i(x,y) u_{y,i} \tag{3}$$

where $N_i(x,y)$ are the shape functions given as follows:

$$N_1(x,y) = \frac{(x-x_2)(y-y_2)}{A} \tag{4}$$

$$N_2(x,y) = -\frac{(x-x_1)(y-y_2)}{A} \tag{5}$$

$$N_3(x,y) = \frac{(x-x_1)(y-y_1)}{A} \tag{6}$$

$$N_4(x,y) = -\frac{(x-x_2)(y-y_2)}{A} \tag{7}$$

$u_{x,i}$ and $u_{y,i}$ are the displacement along *x* and *y* direction, respectively, of the four nodes on the diaphragm unit, whose coordinates are given by: Node 1 (x_1, y_1), Node 2 (x_2, y_1), Node 3 (x_2, y_2), Node 4$((x_1, y_2)$. A is the area of the diaphragm unit.

3.5. Type of Analyses and Related Issues

For each of the archetype buildings considered in this study, modal analysis, nonlinear static pushover analysis, and nonlinear response history analyses were conducted to investigate the behavior of the buildings with different diaphragm design procedures. Some additional details of the analyses are provided in this section.

3.5.1. Modal Analysis

Modal analysis was performed for the archetype buildings in *OpenSees* to obtain their natural periods and mode shapes. Results were compared to structural models in a commercial structural analysis software, *SAP2000*, as discussed in the next chapter.

3.5.2. Nonlinear Static Pushover Analysis

Pushover analysis was conducted to study the static behavior of the archetype buildings. A displacement-controlled load pattern was applied to the structure in the short direction (long diaphragm span direction), where the displacement of the center node on the roof in the short direction controlled the solution. Per FEMA P695, vertical distribution of the lateral force at each node was assigned proportional to the product of the tributary mass and the fundamental mode shape coordinate at the node: $F_x \propto m_x \phi_{1,x}$, where F_x is the relative magnitude of force applied at node x, m_x is the mass associated with node x, and $\phi_{1,x}$ is the fundamental mode shape coordinate at node x. A view of the lateral force distribution on the 4-story archetype building is shown in Figure 13, in which the arrow length denotes the relative magnitude of the applied force.

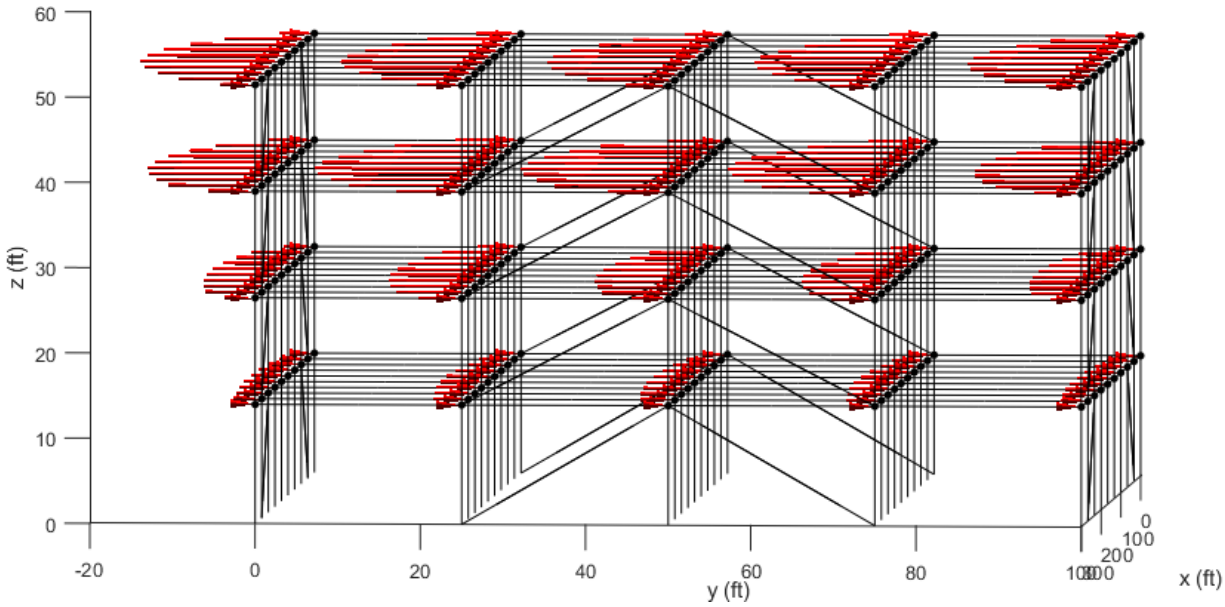

Figure 13 Lateral force distribution on 4-story archetype building for pushover analysis

3.5.3. Nonlinear Response History Analysis

To evaluate the seismic performance of the archetype buildings with different diaphragm design procedures, nonlinear response history analysis was performed with the archetype models subjected to the suite of FEMA P695 far-field earthquake motions. This section provides some details for the scaling of ground motion records to desired hazard levels and the criteria adopted to define building collapse.

3.5.3.1. Ground Motion Scaling

A total of 22 pairs of FEMA P695 far-filed earthquake ground motions (44 records) were used in this study, which were applied in orthogonal directions of the building in the nonlinear response history analysis (two possible orientations of each pair resulted in 44 total sets of analysis for each archetype building model). Information of the 22 ground motion pairs is given in Table 10.

Table 10 Far-Field Ground Motions Used for Nonlinear Response History Analysis

ID No.	Earthquake			Recording Station	
	Magnitude	Year	Name	Name	Owner
1	6.7	1994	Northridge	Beverley Hills - Mulhol	USC
2	6.7	1994	Northridge	Canyon Country - WLC	USC
3	7.1	1999	Duzke, Turkey	Bolu	ERD
4	7.1	1999	Hector, Mine	Hector	SCSN
5	6.5	1979	Imperial Valley	Delta	UNAMUCSD
6	6.5	1979	Imperial Valley	El Centro Array #11	USGS
7	6.9	1995	Kobe, Japan	Nishi-Akashi	CUE
8	6.9	1995	Kobe, Japan	Shin-Osaka	CUE
9	7.5	1999	Kocaeli, Turkey	Duzce	ERD
10	7.5	1999	Kocaeli, Turkey	Arcelik	KOERI
11	7.3	1992	Landers	Yermo Fire Station	CDMG
12	7.3	1992	Landers	Coolwater	SCE
13	6.9	1989	Loma Prieta	Capitola	CDMG
14	6.9	1989	Loma Prieta	Gilroy Array #3	CDMG
15	7.4	1990	Mnajil, Iran	Abbar	BHRC
16	6.5	1987	Superstition Hills	El Centro Imp. Co.	CDMG
17	6.5	1987	Superstition Hills	Poe Road (temp)	USGS
18	7.0	1992	Cape Mendocino	Rio Dell Overpass	CDMG
19	7.6	1999	Chi-Chi, Taiwan	CHY101	CWB
20	7.6	1999	Chi-Chi, Taiwan	TCU045	CWB
21	6.6	1971	San Fernando	LA – Hollywood Star	CDMG
22	6.5	1976	Friuli, Italy	Tolmezzo	-

Three scale levels were considered for nonlinear response history analysis (NRHA): 1) design earthquake (DE), 2) maximum considered earthquake (MCE), and 3) a scale level based on adjusted collapse marginal ratio ($ACMR_{10\%}$, see FEMA P695). The third scale level was considered to evaluate the conformance of the archetype buildings with the acceptance criteria in FEMA P695, i.e., less than 50% of ground motions causing collapse implies conformance with the acceptance criteria.

In this study, Seismic Design Category (SDC) D_{max} from FEMA P695 was considered. The design spectral acceleration parameters, $S_{DS} = 1.0$, $S_{D1} = 0.6$, were used to create the target design earthquake (DE) spectrum. The maximum considered earthquake (MCE) spectrum was obtained using 1.5 times the S_{DS} and S_{D1} values. The third scale level ($ACMR_{10\%}$) is related to median collapse for acceptability according to FEMA P695.

The 44 ground motion records were scaled accordingly to each desired level in the nonlinear response history analysis. For DE and MCE, the ground motions were scaled such that the median spectrum matches the design spectrum at the fundamental period of the building (see Figure 14). To be consistent with FEMA P695 methodology, the value of the fundamental period for each archetype building was obtained by the product of the coefficient for upper limit on calculated period (C_u) and the approximate fundamental period (T_a) as defined in ASCE 7-16 Section 12.8.2, which is provided in Table 3. The scale factor for the third scale level ($ACMR_{10\%}$) was obtained with the method as described in Appendix F.3 of FEMA P695: first an acceptable value of adjusted collapse margin ratio ($ACMR_{10\%}$) was obtained with assumed total system collapse uncertainty; then the period-based ductility (μ_T) was obtained from the pushover analysis; and finally the spectral shape factor (*SSF*) and the collapse margin ratio (*CMR*) was obtained. The scale factor based on $ACMR_{10\%}$ was then obtained by multiplying the collapse marginal ratio by the scale factor for MCE. An example is given below based on 4-story building with traditional diaphragm design. The values for the other buildings are provided in Table 11.

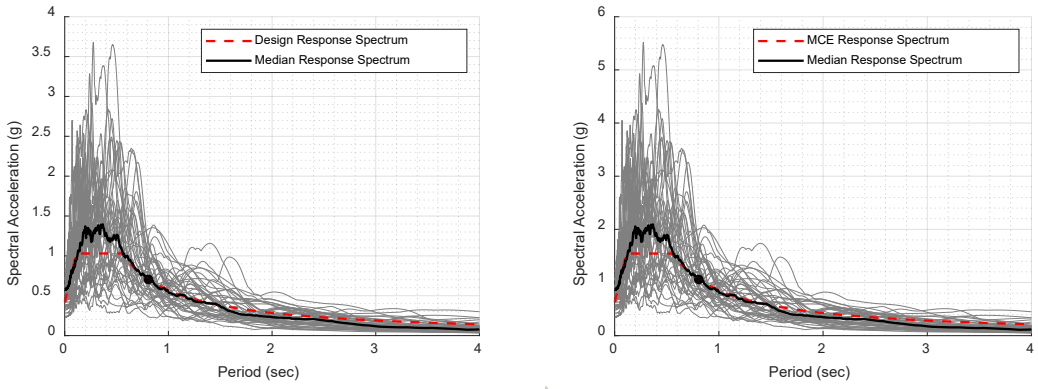

(a) DE (b) MCE

Figure 14 Example ground motion scaling for DE and MCE (4-story building)

Example calculation of $ACMR_{10\%}$ scale factor for 4-story archetype buildings with traditional diaphragm design:

1. Period-based ductility, μ_T, is obtained from the pushover analysis. Values of the coefficient C_0, maximum base shear V_{max}, building weight W, fundamental period T (equal to $C_u T_a$), fundamental period obtained from modal analysis T_1, effective yield roof

drift displacement $\delta_{y,eff}$, ultimate roof drift displacement δ_u, and period-based ductility μ_T, are given as follow (see FEMA P695 for details):

a. $C_0 = 2.03$
b. $V_{max} = 1335$ kip
c. $W = 8930$ kip
d. $T = 0.81$ sec
e. $T_1 = 1.17$ sec
f. $\delta_{y,eff} = 4.06$ in.
g. $\delta_u = 43.29$ in.
h. $\mu_T = 10.65$

2. Assumed total system collapse uncertainty, $\beta_{TOT} = 0.525$, based on the following
   a. Total system collapse uncertainty is calculated based on Equation 7-5 per FEMA P695:
   b. $\beta_{TOT} = \sqrt{\beta_{RTR}^2 + \beta_{DR}^2 + \beta_{TD}^2 + \beta_{MDL}^2}$
      where $\beta_{TOT} =$ total system collapse uncertainty, $\beta_{RTR} =$ record-to-record collapse uncertainty, $\beta_{DR} =$ design requirements-related collapse uncertainty, $\beta_{TD} =$ test data-related collapse uncertainty, $\beta_{MDL} =$ modeling-related collapse uncertainty
   c. Assuming the quality ratings for design requirements, test data, and modeling are all Good, we have (Section 7.3.4): $\beta_{DR} = 0.20$, $\beta_{TD} = 0.20$, $\beta_{MDL} = 0.20$
   d. β_{RTR} is a function of period-based ductility μ_T (Equation 7-2): $\beta_{RTR} = 0.1 + 0.1\mu_T \leq 0.40$, But for $\mu_T \geq 3$, we have $\beta_{RTR} = 0.40$.
   e. $\beta_{TOT} = \sqrt{\beta_{RTR}^2 + \beta_{DR}^2 + \beta_{TD}^2 + \beta_{MDL}^2} = \sqrt{0.40^2 + 0.20^2 + 0.20^2 + 0.20^2} = 0.525$ (rounded to the nearest 0.025). This value can also be obtained directly from Table 7-2b of FEMA P695.
3. Find acceptable level of ACMR: ACMR for 10%
   a. Using Table 7-3 with $\beta_{TOT} = 0.525$, and 10% collapse probability
   b. $ACMR_{10\%} = 1.96$
4. Spectral shape factor, SSF
   a. Table 7-1b of FEMA P695 is used to get SSF

b. Based on period, $T = C_u T_a = 0.81$ sec for BRBF building and period based ductility, $\mu_T = 10.65$

c. $SSF = 1.41$

5. Find scale factor as scale factor for MCE multiplied by CMR

a. The scale factor is obtained using Equation G-1 of FEMA P695:

$$SF_{ACMR_{10\%}} = \frac{ACMR_{10\%}}{C_{3D} SSF}\left(\frac{S_{MT}}{S_{NRT}}\right)$$

$$SF_{ACMR_{10\%}} = \frac{ACMR_{10\%}}{C_{3D} SSF} SF_{MCE}$$

$$SF_{ACMR_{10\%}} = \frac{1.96}{1.2(1.41)} 2.5$$

$$SF_{ACMR_{10\%}} = 2.90$$

Table 11 Ground Motion Scaling for all Buildings

Building	$C_u T_a$ (sec)	T_1 (sec)	μ_T	β_{TOT}	$ACMR_{10\%}$	SSF	DE Scale Factor, SF_{DE}	MCE Scale Factor, SF_{MCE}	$ACMR_{10\%}$ Scale Factor, $SF_{ACRM_{10\%}}$
1-story (bare steel deck roof)	0.30	1.00	7.01	0.525	1.96	1.31	1.29	1.94	2.43
1-story (comp. deck roof)	0.30	0.81	28.18	0.525	1.96	1.33	1.29	1.94	2.39
4-story	0.81	1.17	10.66	0.525	1.96	1.41	1.67	2.50	2.90
8-story	1.34	2.06	5.21	0.525	1.96	1.43	1.67	2.50	2.86
12-story	1.81	2.77	3.51	0.525	1.96	1.36	1.99	2.98	3.58

3.5.3.2. Criteria for Collapse Definition

To perform statistical analysis on building collapse using the nonlinear response history analysis results, it is necessary to determine whether a ground motion caused building collapse based on selected criteria, including non-simulated collapse. For collapse definition in the response history analyses, the three criteria listed in the following were considered, and if any of them was satisfied, the building was considered as collapsed. It should be noted that some limit

states such as BRB fracture were explicitly captured in the models and therefore not included in these criteria.

1) Peak resultant story drift ratio (as defined in Section 3.4.1) exceeds 10%. This limit is consistent with the evaluation of two-dimensional BRBF collapse performance by NIST (Kircher et al., 2010).
2) Maximum diaphragm shear angle exceeds 4%. This limit is determined based on the evaluation of the cantilever diaphragm test and connector test database, in which the majority of the specimens failed at an average shear angle equal to 4%.
3) Convergence failure occurs in the analysis. There are potentially many reasons for convergence failure during the analysis, and one of them is that large displacements cause local or global instability. For those runs of analysis that fail to converge, criteria 1) and 2) are first checked. If neither of these two criteria is met, the time history of story drift at the location where the maximum story drift occurs is examined on a case-by-case basis. Examples for determining the occurrence of building collapse in an individual analysis are provided as follows.

    i) If the building collapses under the same pair of ground motions with a smaller scale factor, then the building is considered collapsing and is included in the calculation of collapse ratio of all runs (with the reasoning that smaller magnitude of ground motions typically cause less damage to the building). Alternative, a run may be considered a collapse if the building undergoes substantial amount of inelastic deformation at the early stage of analysis (e.g. before the peak ground acceleration is applied). Figure 15 shows an example time history of maximum story drift for the runs of analysis with two different scale levels of ground motions. The analysis fails to converge for $ACMR_{10\%}$-level ground motions. However, because the building is considered to collapse for the analysis with the same pair of ground motions at MCE level (the story drift ratio exceeds 10%), it is also considered to collapse for the $ACMR_{10\%}$ level since the ground motions are scaled to a higher hazard level.

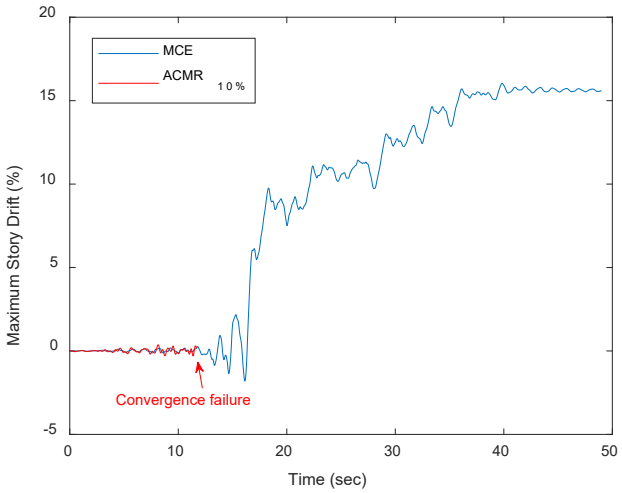

Figure 15 Example time history of maximum story drift for analysis with convergence failure considered as building collapse (4-story Trad. / Alt.2, Ground Motion Set 21)

ii) If the building does not collapse under the same pair of ground motions with a larger scale factor, then the building is considered non-collapsing and is included in the calculation of collapse ratio of all runs. The reasoning is that smaller magnitude of ground motions typically cause less damage to the building.

iii) If it cannot be determined whether the building collapses or not, the run is excluded from the calculation of collapse ratio of all runs. This happens if neither i) nor ii) is satisfied. In this case, the analysis is considered incomplete, and is deemed inappropriate to be included in the calculation of collapse ratio. An example is shown in Figure 16.

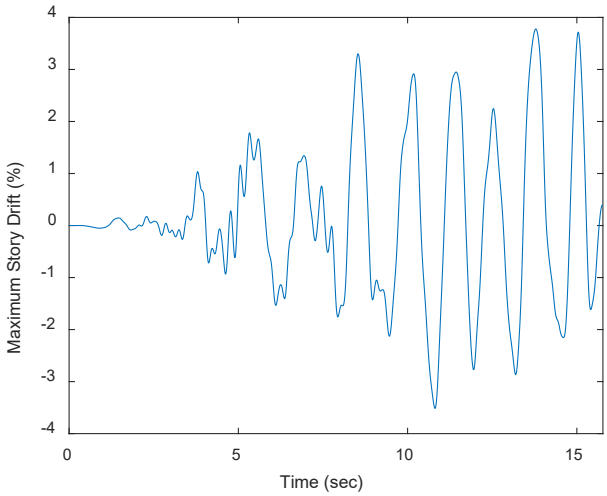

Figure 16 Example time history of maximum story drift for analysis with convergence failure excluded from collapse ratio calculation (8-story Trad. / Alt.2, Ground Motion Set 26)

4. Results and Discussion

4.1. Modal Analysis

Eigenvalue analysis was performed for the archetype buildings to obtain their natural periods and mode shapes. To study the effect of the rigid diaphragm assumption on modal properties of the building structure, linear elastic models were also created using the commercial structural analysis program *SAP2000* for the building framing members using rigid diaphragm constraints. Table 12 provides the 1st and 2nd periods of the archetype buildings obtained from eigenvalue analysis of the models in *OpenSees* that uses an elastic diaphragm and *SAP2000* that uses a rigid diaphragm. The 1-story archetype building with bare steel deck roof has more flexible diaphragm, so the fundamental period is most affected by the rigid diaphragm assumption in SAP model. Other archetype buildings have concrete on steel deck typical floor diaphragms (more rigid) so the periods are less affected. Figure 17 shows the mode shape for the 1st mode of the four-story archetype models. It can be observed that diaphragm deflections can have a substantial effect on building natural period (up to 48% larger than rigid) and on the mode shape shown in Figure 17a which shows potential for a "whipping effect" at the roof due to roof diaphragm flexibility. Different mode shapes of the 4-story archetype building are also shown in Figure 18.

Table 12 Natural Periods of Archetype Models in OpenSees and SAP2000

Building Model	Long Dimension Mode 1 (sec)			Short Dimension Mode 1 (sec)		
	Elastic Diaphragm (OpenSees)	Rigid Diaphragm (SAP)	Difference	Elastic Diaphragm (OpenSees)	Rigid Diaphragm (SAP)	Difference
1-story (bare steel deck roof)	0.61	0.46	25%	1.00	0.52	48%
1-story (concrete on steel deck roof)	0.81	0.53	35%	0.61	0.41	33%
4-story	1.17	0.94	20%	1.17	0.76	35%
8-story	2.61	1.79	31%	1.84	1.40	24%
12-story	2.77	2.41	13%	2.38	1.91	20%

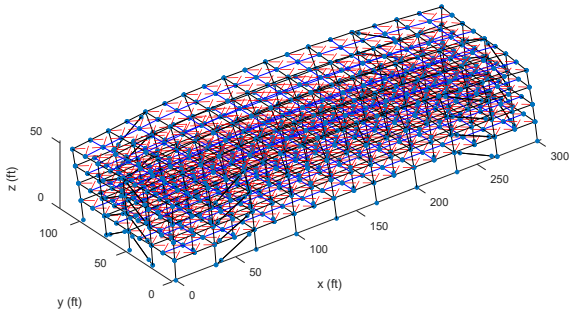

(a) OpenSees model

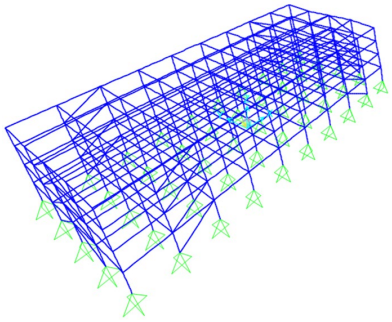

(b) SAP2000 model

Figure 17 Mode shapes for the 1st mode of four-story archetype models

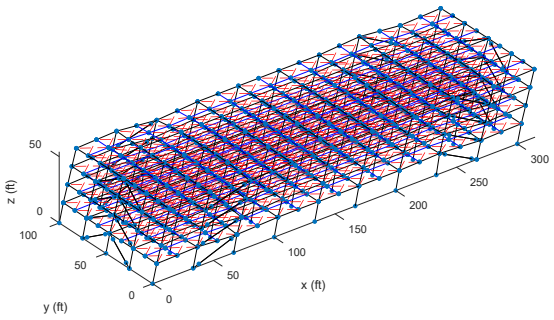

(a) Long dimension Mode 1 (T = 1.17 sec)

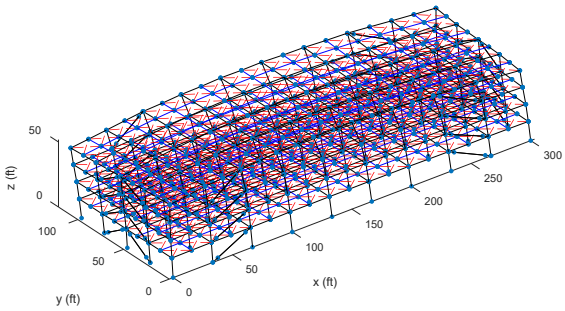

(b) Short dimension Mode 1 (T = 1.17 sec)

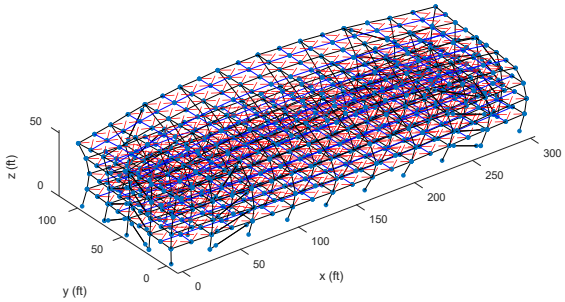

(c) Short dimension Mode 2 (T = 0.74 sec)

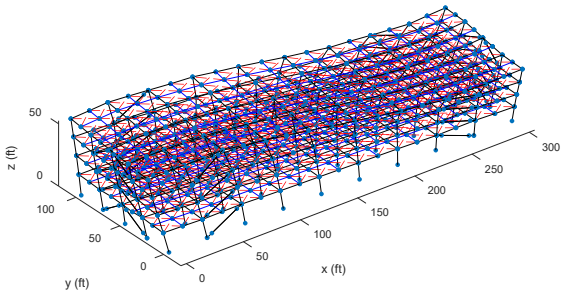

(d) Torsional mode (T = 0.61 sec)

Figure 18 Mode shapes of four-story archetype models

4.2. Nonlinear Static Pushover Analysis

Pushover analysis was conducted to study the static behavior of the archetype buildings. Figure 19 shows the pushover curves of the archetype buildings with different diaphragm designs. The drift ratio was calculated as the applied displacement at the center of the roof divided by the

building height. It can be observed that the different diaphragm designs had little effect on the pushover behavior because the pushover analyses were dominated by BRB inelasticity. The load pattern was based on the first mode shape and for these buildings resulted in BRB yielding instead of diaphragm inelasticity. The first point of nonlinearity on the pushover curves is associated with yielding of the BRB cores, followed by a hardening segment with reduced slope, which is related to the stiffness provided by the BRB frames before hinging occurs at the beam-to-column connections. This is more pronounced for the 1-story and 4-story buildings. Once the beam-to-column connections develop plastic hinges, softening response occurs due to P-Δ effect (note that the analysis for 4-story building with Traditional / Alternative 2 diaphragm design failed to converge before secondary softening occurred). Secondary hardening is not observed for the 8 and 12-story models where P-Δ effect controls over the BRB material hardening after the peak load.

The deformed shapes of the building models at the end of the pushover analysis are shown in Figure 20. As the behavior of the buildings were dominated by the BRB inelasticity, diaphragm deformation was not observable in the deformed shape, while the story drift of the buildings primarily concentrated in the first several stories from the ground level.

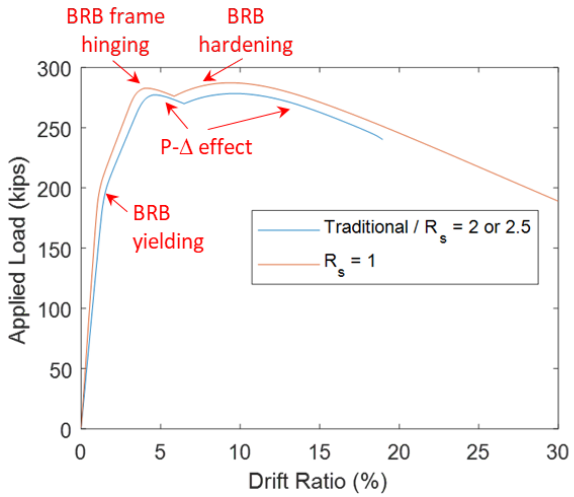

(a) 1-story with bare steel deck roof

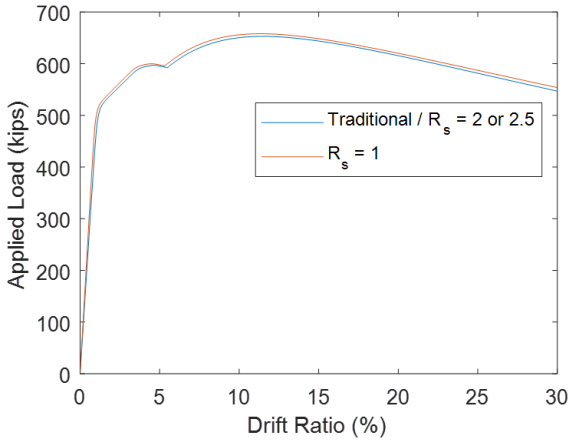

(b) 1-story with composite concrete on steel deck roof

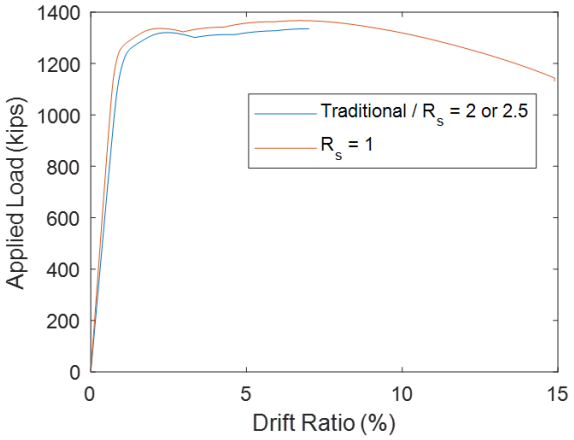

(c) 4-story

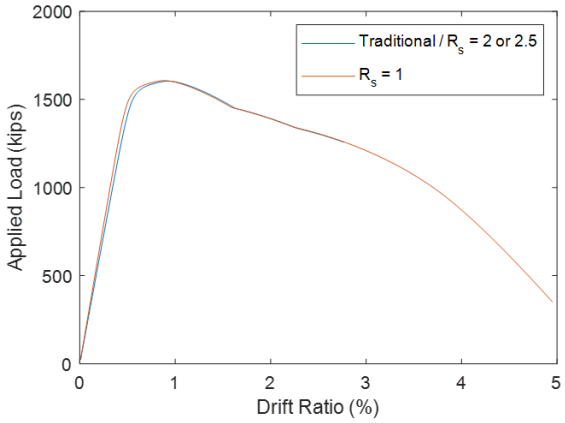

(d) 8-story

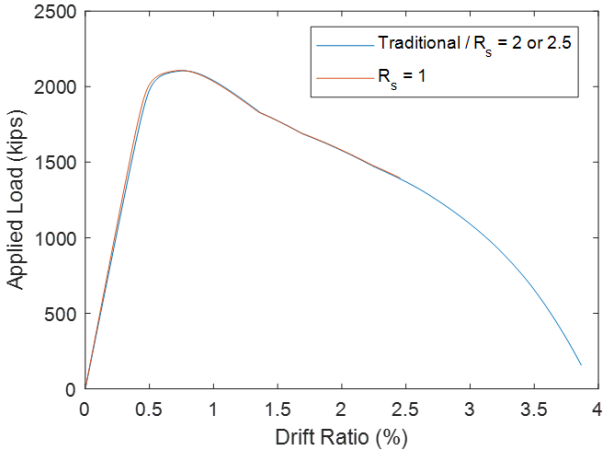

(e) 12-story

Figure 19 Pushover curves of archetype buildings with different diaphragm design procedures

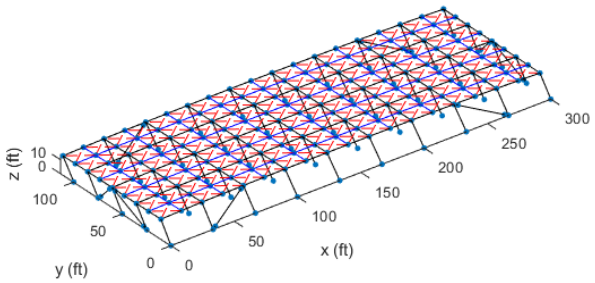

(a) 1-story (bare steel deck roof)

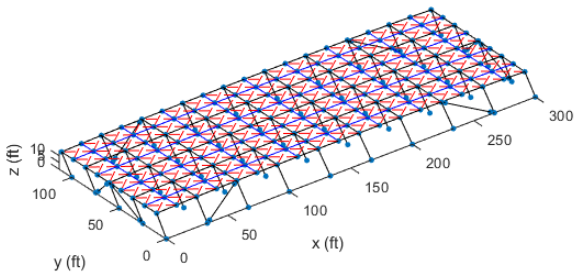

(b) 1-story (composite concrete on steel deck roof)

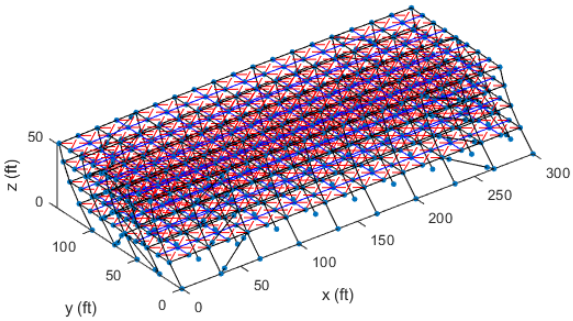

(c) 4-story

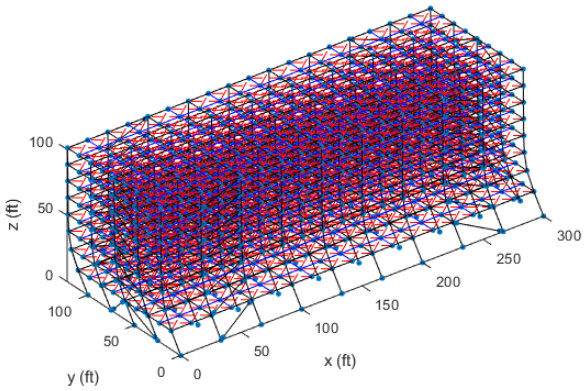

(d) 8-story

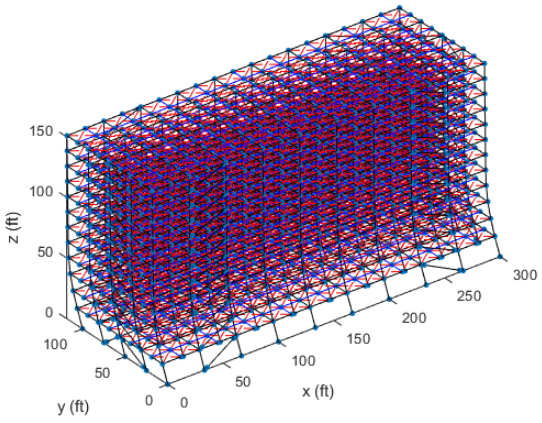

(e) 12-story

Figure 20 Deformed shapes of archetype buildings with Trad. or Alt. 2 diaphragm design procedures (deformation amplification factor: 5)

4.3. Nonlinear Response History Analysis

To evaluate the seismic performance of the archetype buildings with different diaphragm design procedures, nonlinear response history analysis was performed with the archetype

models subjected to the suite of FEMA P695 far-field earthquake motions scaled to different hazard levels. Results of the analysis is presented in this section.

4.3.1. Detailed Investigation of 4-story Building Behavior Subjected to One Ground Motion Pair

This section provides a detailed investigation of building behavior in the nonlinear response history analysis using a single building height subjected to one ground motion pair. The 4-story archetype building model with different diaphragm designs subjected to the ground motion with ID No. 7 in Table 10 at different earthquake hazard levels was selected.

Figure 21 shows response history results including peak story drift (at the location where the maximum story drift ratio occurred), BRB hysteresis (at the location where the maximum BRB force occurred), and diaphragm truss hysteresis (at the location where the maximum diaphragm shear angle occurred) of the buildings with Traditional / Alternative 2 diaphragm design. While the peak story drift of the building subjected to DE-level ground motion is less than 3%, the MCE-level ground motion produces peak story drift larger than the 10% limit for collapse definition, and under $ACMR_{10\%}$-level ground motion the building experiences ever increasing story drifts, which indicates building collapse. The BRB's and diaphragms both undergo inelastic deformation at all three hazard levels. For BRB's, the hysteresis curves show that energy is dissipated by the BRB inelastic deformation, and at the $ACMR_{10\%}$ level, excessive BRB deformation occurs and causes the building to collapse. Floor diaphragms remain relatively elastic compared to the roof diaphragms under the DE and MCE-level ground motions, whereas at the $ACMR_{10\%}$ level, the floor diaphragms are affected by the large story drift due to the excessive deformation of the BRB and also undergo large deformation.

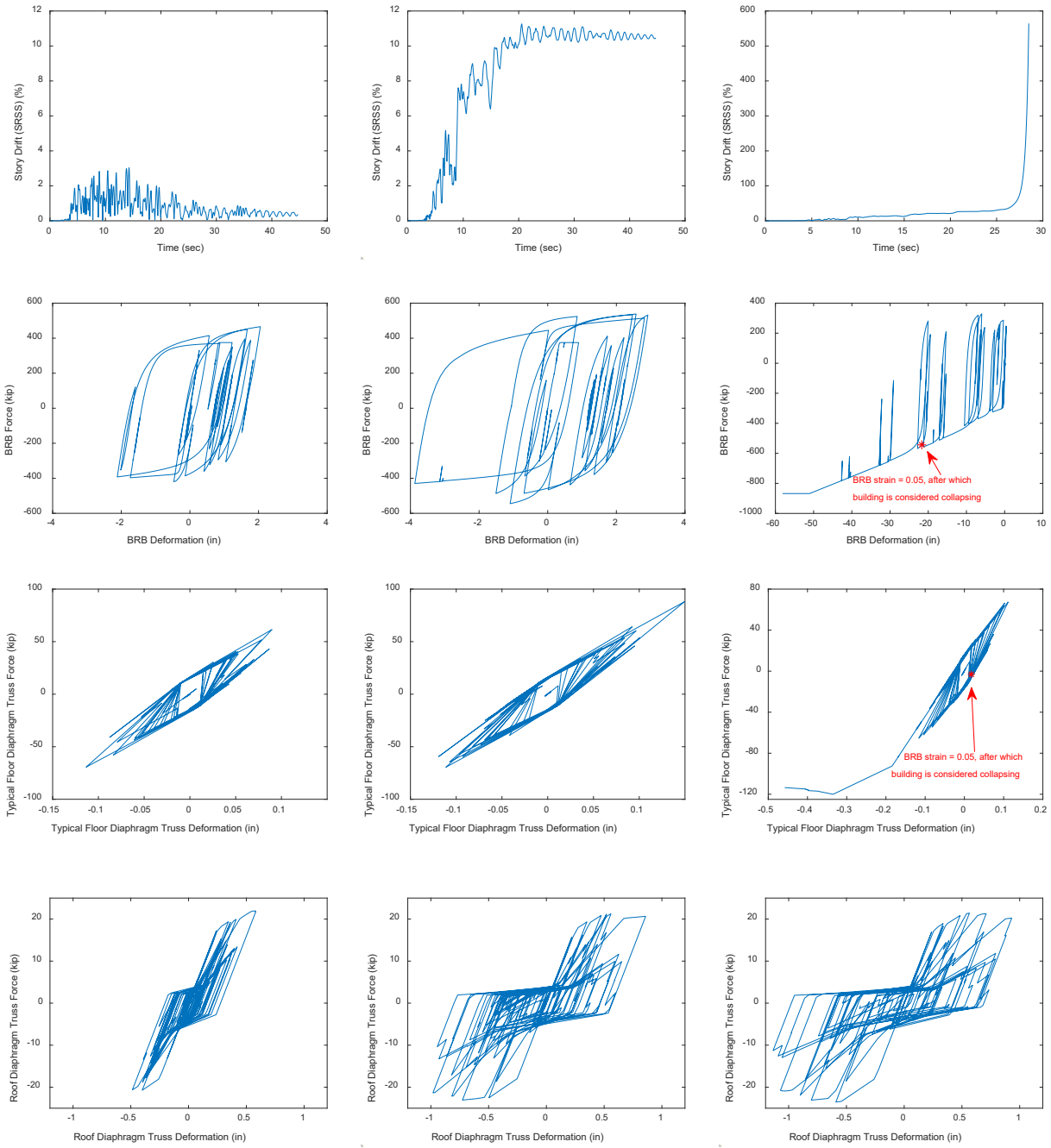

(*a*) DE (*b*) MCE (*c*) $ACRM_{10\%}$

Figure 21 Time history response of 4-story building with the Traditional / Alternative 2 diaphragm design under three levels of ground motions (from top to bottom: peak story drift, base story BRB hysteresis, floor diaphragm truss hysteresis, roof diaphragm truss hysteresis)

Figure 22 shows the deformed shapes of the building under the three levels of the ground motion (plotted at the moment in the time history when peak story drift occurs). The deformed

shapes further illustrate the cause of building collapse at the MCE and $ACMR_{10\%}$-level ground motions which is failure of BRB's, particularly at the first story where story drifts concentrate. In addition, unlike the first-mode based pushover analysis in which inelasticity focuses in the BRB's, the participation of higher modes in the response history analysis leads to diaphragm inelasticity. The total story drifts include inelastic deformations in the vertical LFRS and the diaphragm such that the two compound each other (i.e. interact) to exacerbate the P-Δ effect which eventually leads to the collapse of the buildings.

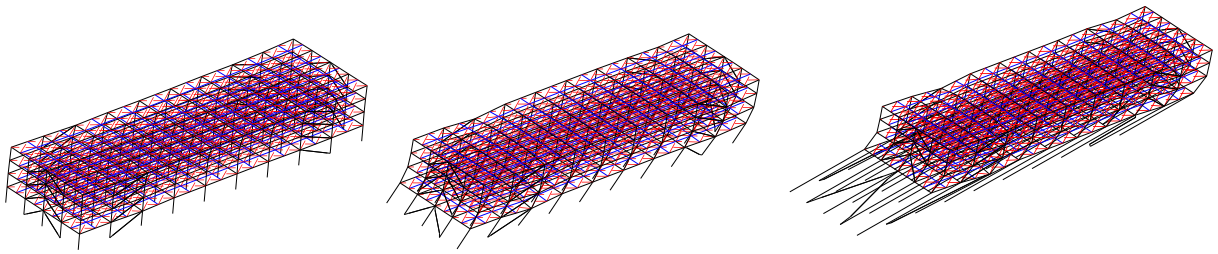

(*a*) DE (*b*) MCE (*c*) $ACRM_{10\%}$

Figure 22 Deformed shapes of 4-story archetype building with the Traditional / Alternative 2 diaphragm design under three levels of ground motions (deformation amplification factor: 10)

Figure 23 shows the time history of the maximum total story drift (at any location of the building including diaphragm deformation) and the maximum story drift at the BRB frames plotted separately for the x (along the longer dimension of the building) and y (along the shorter dimension of the building) directions of the archetype building with Traditional / Alternative 2 diaphragm design subjected to the ground motion at MCE level. It can be observed that the building experiences larger story drift in the x direction than in the y direction, possibly because the magnitude of ground motion accelerations is larger in the x direction than in the y direction. Also, the total story drift in the x direction is very close to the story drift at the BRB frames throughout the time history, indicating negligible in-plane diaphragm deformation in this direction, which is due to the large in-plane stiffness of the diaphragm along the longer dimension of the building. However, the in-plane stiffness of the diaphragm in the y direction is much smaller, resulting in significantly larger in-plane diaphragm deformations and thus the total story drift is substantially larger than the story drift at the BRB frames in this direction. This is worth some attention as in conventional structural analysis where diaphragms are assumed infinitely

rigid or elastic in plane with zero or small deformation, the story drift of the building could be underestimated.

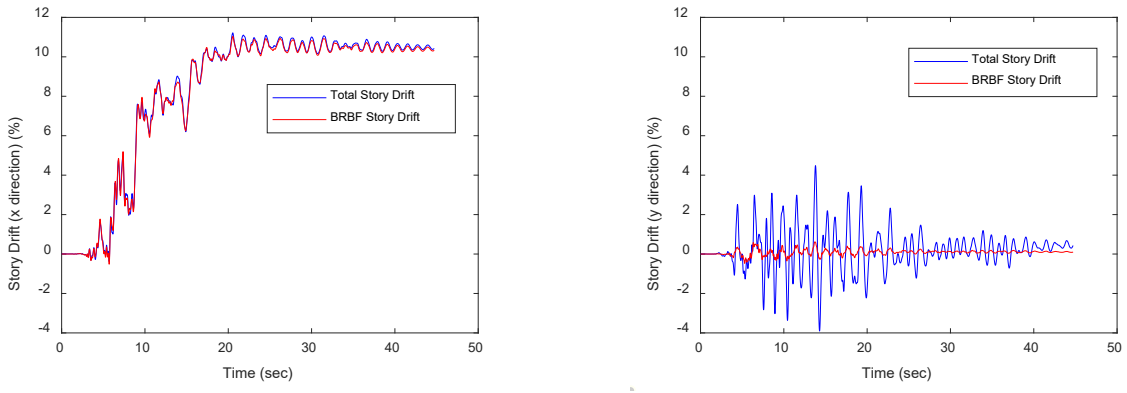

(a) x direction (long direction) (b) y direction (short direction)

Figure 23 Time history of peak story drift in x and y directions of 4-story building with Traditional / Alternative 2 diaphragm design under MCE-level ground motion: total story drift vs. BRBF story drift

Figure 24 shows the time history of the maximum total base shear (including the shear in the columns at the base story) and the maximum base shear at the BRB frames plotted separately for the x and y directions of the 4-story archetype building with Traditional / Alternative 2 diaphragm design subjected to the ground motion at DE and MCE levels. The peak values of these base shears are provided in Table 13. It can be observed that although the scale factor for MCE ground motion accelerations is 1.5 times larger than that for DE ground motions, the peak base shear is an average of 1.2 times larger for MCE compared to DE because the BRBF strength limits the force that can transfer through the vertical LRFS. It is also noted that the peak total base shear in the y direction is close to the peak base shear at the BRB frames, while in the x direction these two quantities are approximately 40% different, with the peak total base shear being smaller than the peak base shear at the BRB frames. The main reason is that the P-Δ effect causes shear at the base of gravity columns that acts in the direction opposite to the BRBF base shear. From Figure 23 it is shown that the story drift in the x direction is much larger than that in the y direction, and therefore the base shears are more affected by the P-Δ effect, leading to larger difference between the total base shear and BRB frame base shear as shown in Figure 24 and Table 13.

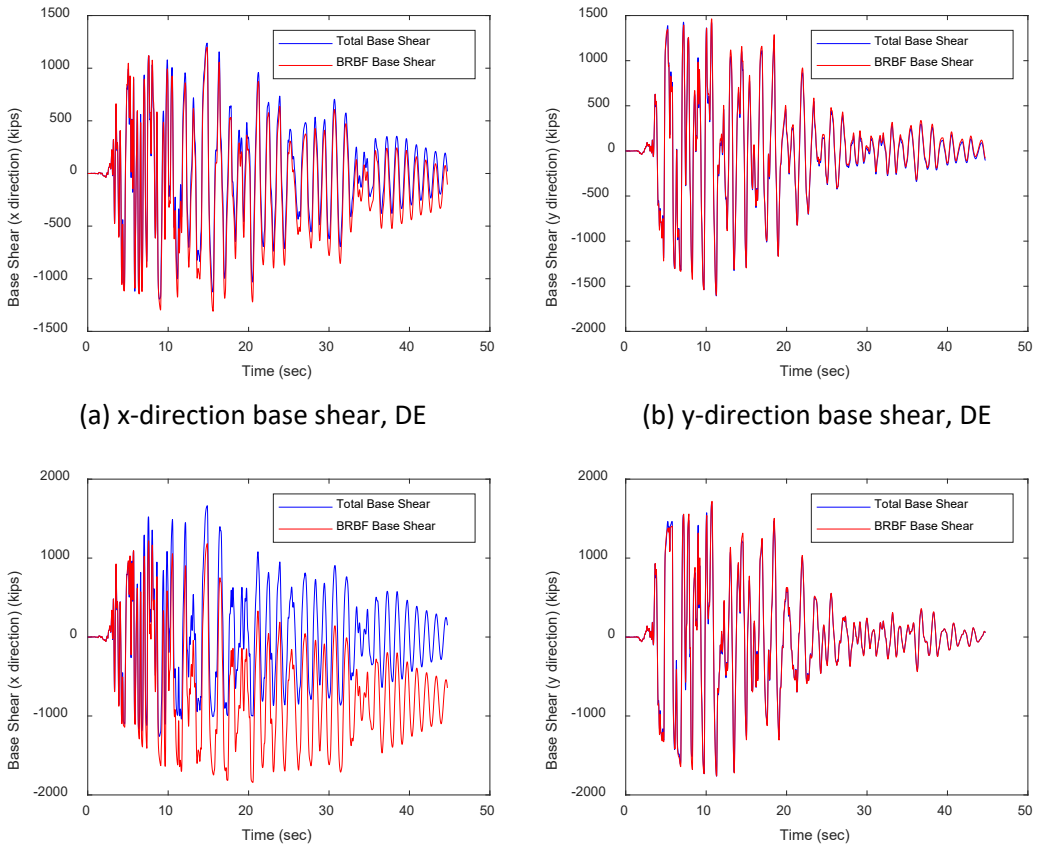

(a) x-direction base shear, DE

(b) y-direction base shear, DE

(c) x-direction base shear, MCE

(d) y-direction base shear, MCE

Figure 24 Example time history of base shear in x and y directions of 4-story building with Traditional /Alternative 2 design under DE and MCE-level ground motions: total base shear vs. BRBF base shear

Table 13 Base Shear of 4-story Archetype Building with Traditional / Alternative 2 Diaphragm Design under DE and MCE-level Ground Motions

Ground motion scale	Peak total base shear in x direction (kip)	Peak BRBF base shear in x direction (kip)	Peak total base shear in y direction (kip)	Peak BRBF base shear in y direction (kip)
DE	1238	1309	1607	1600
MCE	1664	1816	1762	1760

Figure 25 shows the total base shear vs. story drift (of the location where peak story drift occurs) hysteretic curves of the building under the MCE-level ground motion. It is noted that the peak base shear typically does not occur at the same time as the peak story drift, which are both selected for further investigation.

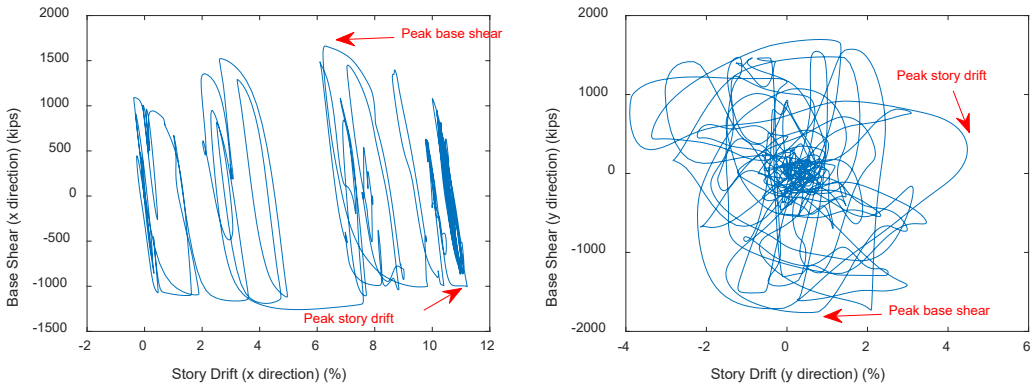

Figure 25 Base shear vs. story drift hysteretic curves of 4-story building with Traditional / Alternative 2 diaphragm design under MCE-level ground motion

Figure 26 shows the contour of the normalized shear angles of the diaphragm units and the normalized strain of the BRB's plotted at different moments in the time history, i.e., at peak story drift and peak base shear in the x and y directions. The y-direction displacement appears small in the contour plotted at the peak story drift because the story drifts in the y direction are much smaller than those in the x direction, as shown in Figure 23. The diaphragm shear angles (γ_{diaph}) are normalized by γ_1, which is the shear angle reached when the diagonal trusses of the diaphragm unit undergo an axial strain equal to ε_1 of the Pinching4 parameters given in Table 5, i.e., the elastic regime. The normalized strain demand of each BRB is obtained by dividing the BRB strain (ε_{BRB}) by ε_y, which is the yield strain of the BRB given by $\varepsilon_y = F_y/E$ where F_y is the yield stress of the BRB and E is the elastic modulus of steel. The normalization is done such that the contours provide a visualization of the inelasticity distribution for the horizontal and vertical systems. It can be observed from Figure 26 that the diaphragm deformation is relatively small at the moment when the peak story drift or the peak base shear in the x direction is reached, but almost all the BRB's parallel to the x-z plane have yielded. However, at the moment when the peak story drift or peak base shear in the y direction occurs, there is significant inelastic deformation in the roof diaphragm and it is concentrated at its two edges where the shear demand is largest.

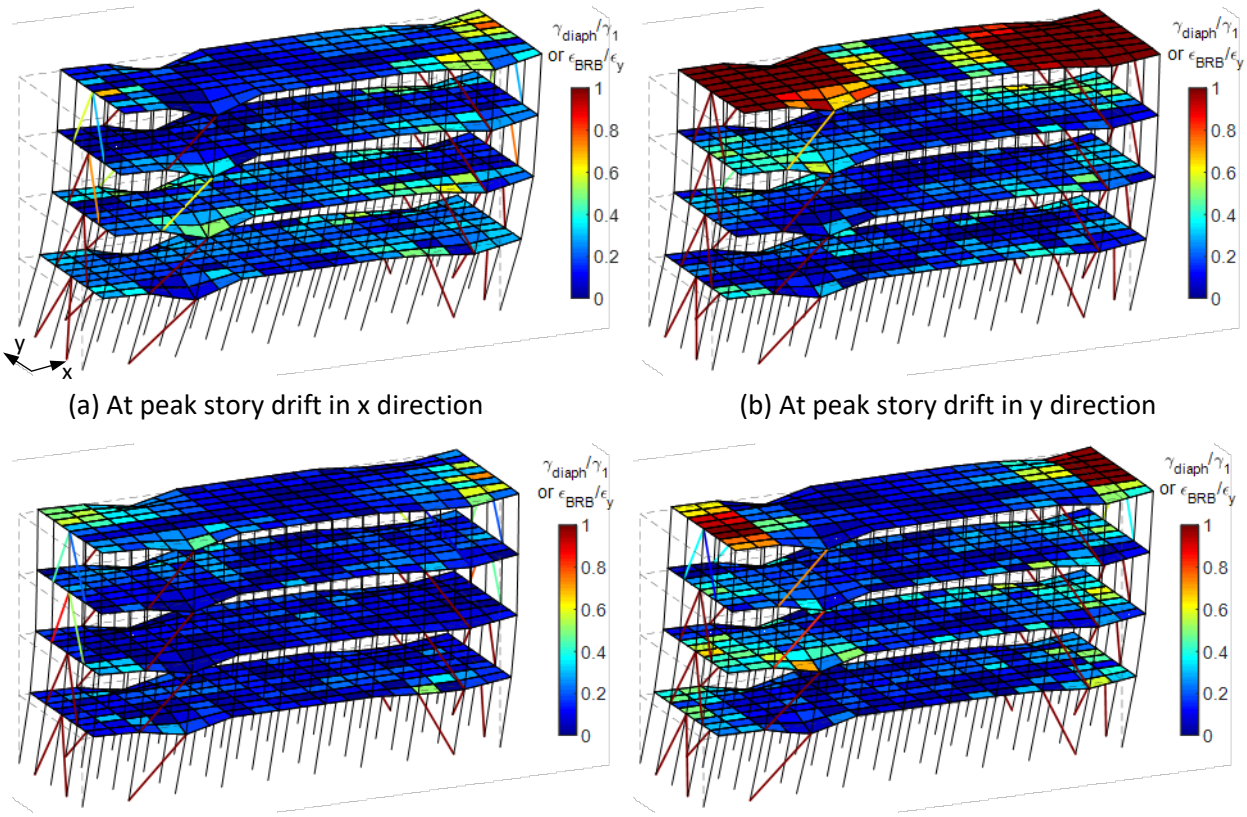

(a) At peak story drift in x direction

(b) At peak story drift in y direction

(c) At peak base shear in x direction

(d) At peak base shear in y direction

Figure 26 Contour of normalized diaphragm shear angle and normalized BRB strain of 4-story building with Traditional / Alternative 2 diaphragm designs under MCE-level ground motion

To illustrate the deformation demands for buildings with different diaphragm designs, the contour of normalized diaphragm shear angle demand and BRB strain demand are plotted in Figure 27. The diaphragm shear angles and BRB strains are normalized as described previously for Figure 26, but in this plot, the maximum deformation demands at any time during the record are used. It can be observed from Figure 27 that in each of the four cases, all the BRB's experienced inelastic deformation. As expected, the diaphragm shear angle demand of the building with Traditional / Alternative 2 diaphragm design was larger than that of the building with Alternative 1 design. Inelastic deformation occurred in the bare steel deck roof diaphragm in each of the four cases, while the composite concrete on steel deck floor diaphragms stayed mostly elastic except that at the MCE level, the floor diaphragms with Traditional / Alternative 2 design exhibited some inelastic deformation demand.

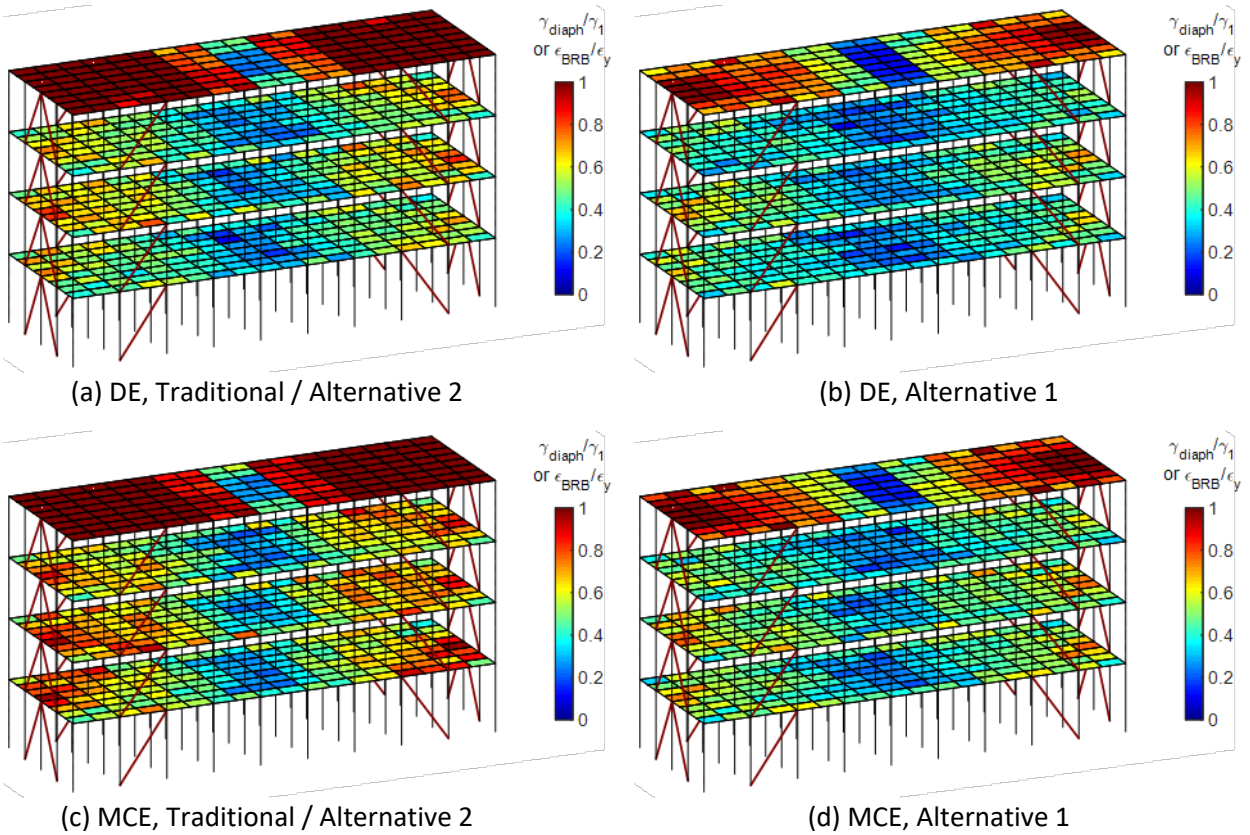

(a) DE, Traditional / Alternative 2

(b) DE, Alternative 1

(c) MCE, Traditional / Alternative 2

(d) MCE, Alternative 1

Figure 27 Contour of normalized diaphragm shear angle demand and normalized BRB strain demand of 4-story building with different diaphragm designs under DE and MCE-level ground motions

4.3.2. Statistical Results and Discussion of All Archetype Buildings

After the results of the nonlinear response history analysis were collected, statistical analysis was performed to investigate the overall seismic behavior and performance of the archetype buildings. Results are provided and discussed in this section.

4.3.2.1. Story Drift

Figure 28 shows an example of the distribution of median peak story drifts at each story along the building height for the 12-story archetype buildings with Traditional / Alternative 2 diaphragm design. The medians of peak story drifts across the 44 runs of analyses was found for each story in the x and y directions for the BRBF frame and the total BRBF plus diaphragm deflection, and for the resultant story drift. One can tell how many cases of the ground motions cause building collapse based on the story drift criterion by counting the number of curves hitting the 10% story drift limit.

It is noted from Figure 28 that the median resultant story drift is larger than the median story drift in the x or y direction alone, especially at the first story where the difference can range approximately from 50% to 100%. When examining x and y story drifts separately, results are similar to planar frame analysis with results close to what can be expected based on the story drift limit per ASCE 7, which is 2% at DE and 3% at MCE. However, the resultant story drift is larger leading to median story drift as large as 3% at DE and 6% at MCE. This indicates that analysis of 2D frames can substantially underestimate peak story drifts.

Since the P-Δ effect is controlled by the story drift in any direction, the resultant story drift is a better estimate of story drift contributing to the P-Δ effect than the x or y-direction story drift considered alone which is typically used in conventional frame analysis. This deserves some attention as there is concentrated story drift at the base story where the gravity load is the largest and thus the P-Δ effects are also the worst. Above the first story along the building height, the story drifts are more uniformly distributed with a smaller magnitude in the intermediate stories, while the story drifts near the roof become larger due to the participation of higher modes. For the BRB frames, the story drifts at the BRB frames in the y direction are typically smaller than those in the x direction. This can be explained by the fact that on one hand, the in-plane stiffness of the diaphragms in the x direction is much larger than in the y direction, forcing more inelasticity to occur in the BRB frames, and on the other hand, the more flexible diaphragms in the y direction can dissipate more energy through inelastic deformation, which reduces the story drifts of the BRB frames in this direction. It can also be observed that because of the different in-plane stiffness of the diaphragms in different directions, the peak total story drifts considering diaphragm deformation are up to 80% larger than the peak story drifts at the BRB frames in the y direction, while in the x direction these two are very close to each other (up to 11% difference), indication much diaphragm deformation in the y direction and little in the x direction. For the same reason, the higher mode effect is more pronounced and causes a much larger difference between the total story drifts and the BRB frame story drifts near the roof.

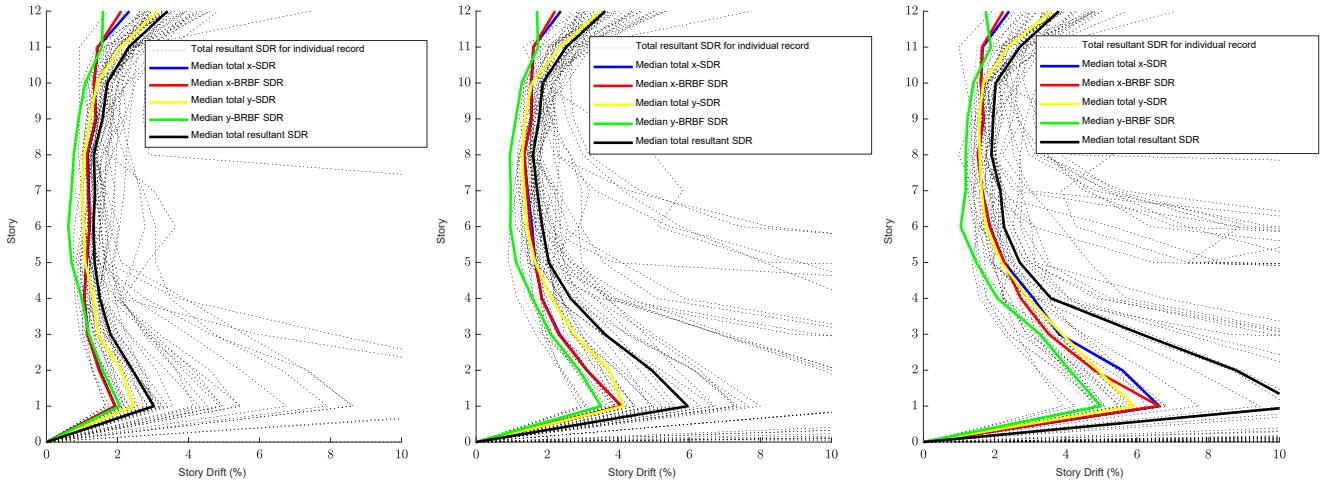

(a) DE (b) MCE (c) $ACMR_{10\%}$

Figure 28 Distribution of median peak story drifts at each story along building height of 12-story archetype buildings with Trad. or Alt. 2 design under three levels of ground motions

Figure 29, 30 and 31 show the distribution of median peak resultant story drift, median peak story drift in the x direction, and the median peak story drift in the y direction along the building height, respectively, for all the archetype buildings under the three levels of ground motions. Values for these quantities are provided in Table A-5 of the Appendix. A similar pattern is observed for the distribution of peak story drift for all the buildings, with larger story drift at the first story, more uniform and smaller story drift at the intermediate stories, and larger story drift near the roof. Due to the 3D effect of the analysis, the median peak resultant story drifts range from 3% for buildings under DE-level ground motions, to approximately 10% for buildings under $ACMR_{10\%}$-level ground motions. If peak story drifts are considered for x or y direction separately, they are reasonably smaller and comparable to results from conventional 2D frame analysis (Chen, 2010; Özkılıç et al., 2018), ranging from slightly larger than 2% for buildings under DE-level ground motions to approximately 6% for buildings under $ACMR_{10\%}$-level ground motions. It can also be observed that different diaphragm design procedures for the archetype buildings do not affect the median peak story drifts much (with an average difference equal to 6%), mainly because the story drifts of the buildings are dominated by the BRB behavior. Another observation is that the median peak story drift at the first story remains similar for all the archetype buildings except for the 12-story building under $ACMR_{10\%}$-level ground motions.

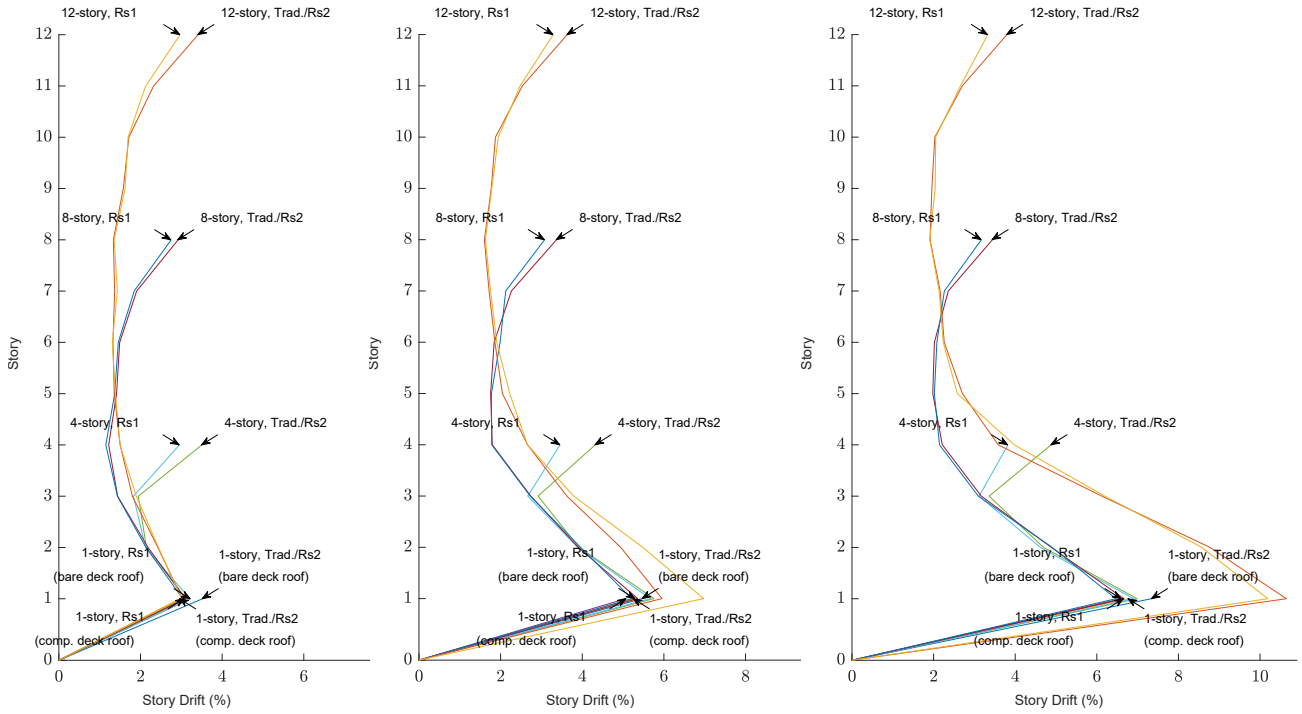

(a) DE (b) MCE (c) $ACMR_{10\%}$

Figure 29 Distribution of median peak resultant story drift along building height

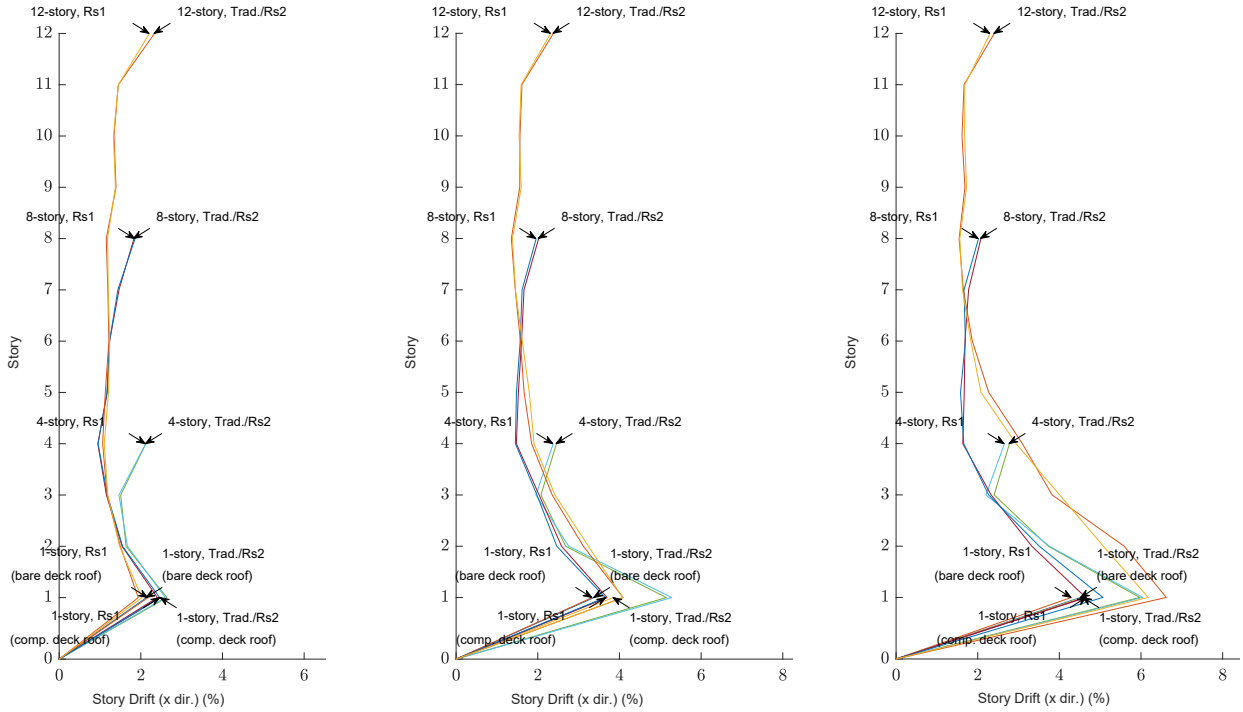

(a) DE (b) MCE (c) $ACMR_{10\%}$

Figure 30 Distribution of median peak story drift in x direction along building height

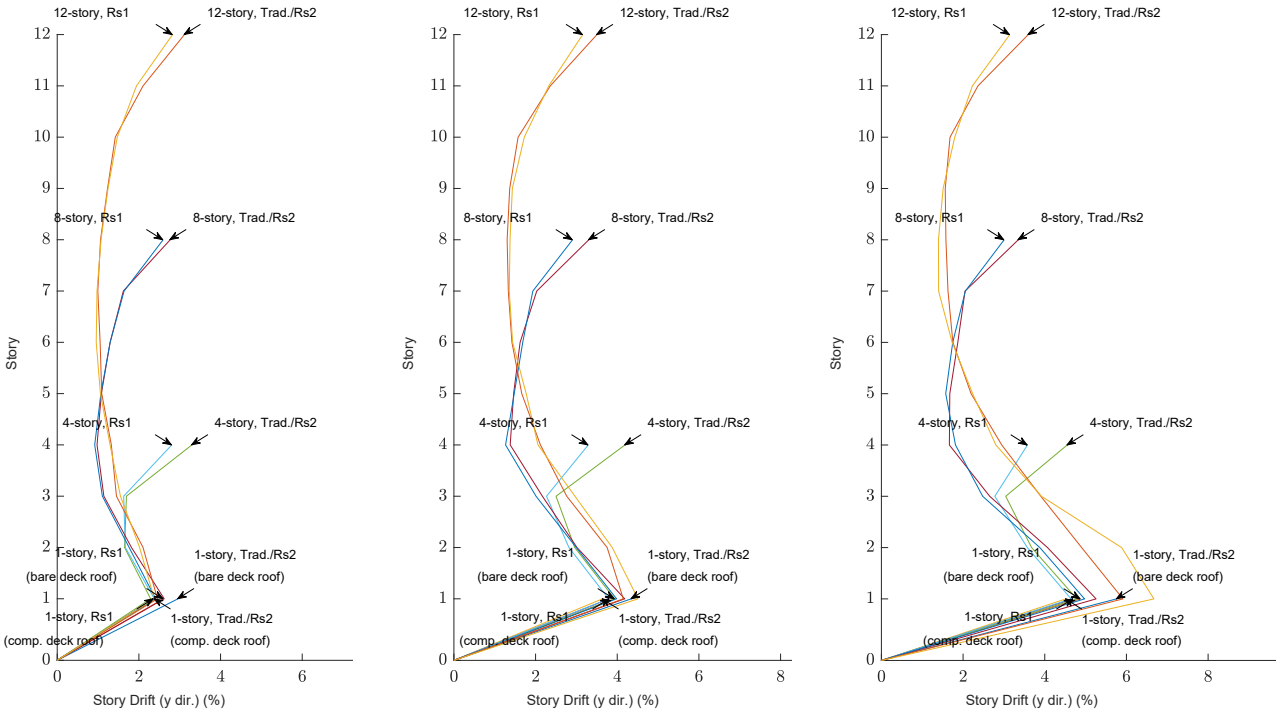

(a) DE (b) MCE (c) ACMR$_{10\%}$

Figure 31 Distribution of median peak story drift in y direction along building height

4.3.2.2. Elastic Diaphragm Shear

To evaluate the accuracy of elastic diaphragm forces from alternative diaphragm design procedure of ASCE 7-16 Section 12.10.3, the diaphragm shear was obtained from the analyses with Alternative 1 diaphragm design procedure (where R_s = 1.0 implies diaphragms should remain elastic). Specifically, the medians of the diaphragm shear demand at the edges, F_{peak}, as calculated by the maximum value of the sum of diaphragm shear along the two edges (x or y direction) in the records, were obtained from the analysis results and provided in Table 14 for each story of the 4-story archetype building. Values for other archetype buildings are given in Table A-6 of the Appendix. These values can be viewed as the median peak inertial forces of the diaphragms. As is shown by the contour of diaphragm deformation demand in Figure 27, the diaphragms of the 4-story building with Alternative 1 diaphragm design remained almost entirely elastic under the DE-level ground motions, and therefore the diaphragm shear demands should be comparable to the elastic design shear for diaphragms F_{px} calculated using the alternative

diaphragm design procedures. It is observed that ratios of the elastic diaphragm shear demand obtained from the analysis to the design shear given by the Alternative 1 diaphragm design procedures are relatively close to 1.0, indicating a reasonable accuracy of the prediction of elastic diaphragm shear demand with the design approach. This can be further validated by the average value of $(F_{peak})_{DE}/F_{px}$ equal to 0.84 for all the archetype buildings. These ratios are shown in Figure 32, and one can also observe that the ratio for the roof diaphragm is the largest among the building stories and in some cases is slightly greater than 1.0 (e.g., 1.06 and 1.03 for the roof of 4-story and 12-story building, respectively). It is therefore concluded that the alternative diaphragm design procedure in ASCE 7-16 produced elastic diaphragm design forces that were somewhat conservative on average, but slightly unconservative at the roof for these archetype buildings with flexible roof diaphragms.

Table 14 Medians of Diaphragm Shear Demand for 4-story Archetype Buildings and Comparison to Design Shear

Diaphragm Design	Story	Median of F_{peak} at DE (kip)			F_{px} (kip)	$\frac{(F_{peak})_{DE}}{F_{px}}$
		x	y	x or y		
Alt. 1	1	746	655	816	977	**0.83**
	2	662	773	796	914	**0.87**
	3	613	629	727	850	**0.86**
	4	352	441	442	419	**1.06**

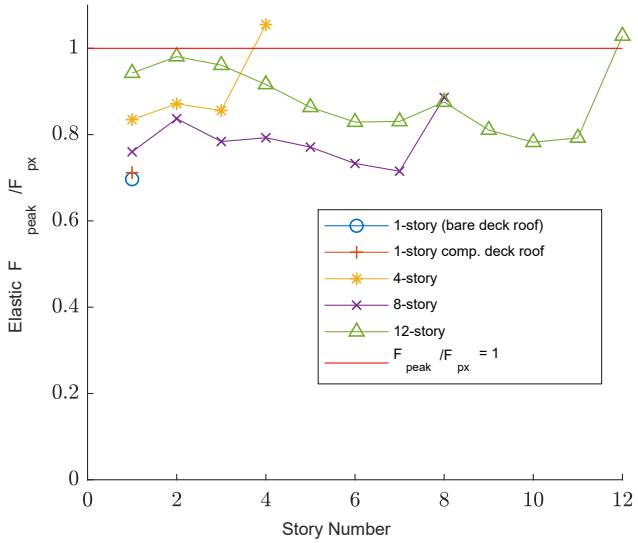

Figure 32 Diaphragm shear demand of archetype buildings with Alternative 1 diaphragm design normalized by diaphragm design shear

4.3.2.3. Collapse Ratio

To investigate the seismic performance objective related to collapse prevention, collapse ratios, i.e., percentage of ground motions causing collapse, were calculated for each set of nonlinear response history analyses. The criteria for defining collapse was given in Section 3.5.3.2. It should be noted that based on collapse criteria item 3) in Section 3.5.3.2, 4 out of 440 runs at DE and 1 out of 440 runs at $ACMR_{10\%}$ with convergence failure in the analysis were excluded from the collapse ratio calculation. The number of analysis runs that are are included in each collapse ratio are given in Table 15, which also provides the collapse ratios for all the archetype buildings.

Figure 33 shows the breakdown of collapse ratios based on each of the three criteria as defined in Section 3.5.3.2, namely, the peak resultant story drift ratio exceeding 10%, the maximum diaphragm shear angle exceeding 0.04 rad., and convergence failure occurring in the analysis. The resulting collapse ratio based on the union of the three collapse criteria is also shown in Figure 33, where the horizontal axis shows the 10 archetype buildings investigated in this study, and the vertical axis is the percentage of ground motions causing collapse. Observations from analysis of the results include the following:

1) As the number of stories increases, collapse ratio of the archetype buildings tends to become larger. This is more pronounced when comparing the 1-story buildings to other multistory buildings subjected to the DE and MCE-level ground motions: under DE-level ground motions, none of the 1-story buildings collapsed, while 6% of the ground motions caused collapse of the multistory buildings; and under MCE-level ground motions, 4% of the ground motions caused collapse of the 1-story building, while 25% of ground motions caused collapse of the multistory buildings. This observation is contrary to findings from some studies where 2D frame analysis was performed and low-rise buildings were deemed more vulnerable. For example, in Kircher et al. (2010), 2-story BRBFs had ACMR values close to 2.0, which was smaller than other BRBFs (with 3 to 16 stories) with ACMR values all larger than 3.0, indicating a smaller collapse margin for short buildings. In another study by Zaruma and Fahnestock (2018), the ACMR value increased from 1.87 for the 4-story baseline BRBF prototype to 2.08 for the 15-story. However, there also exist

some studies which yield a similar conclusion that shorter buildings outperform taller buildings in terms of collapse prevention. In Veismoradi et al. (2016), the target spectral acceleration at the 5%-damped first mode period, $S_a(T_1, 5\%)$, that caused global dynamic instability of the structure decreased from 2.19g for the 3-story BRBF to 1.30g for the 10-story BRBF, indicating a higher capacity to prevent collapse for shorter buildings. Similarly in Khorami et al. (2017), the median value of $S_a(T_1, 5\%)$ associated with the collapse prevention limit state decreased from 2.08g for 3-story BRBF to 0.93g for 10-story BRBF. Further study is warranted to investigate the difference in these results.

2) In terms of collapse ratio, buildings with Alternative 1 diaphragm design perform slightly better than buildings with Traditional / Alternative 2 design, with an average difference of collapse ratios equal to 1.4%, 2.7%, and 2.5% at the DE, MCE, and $ACMR_{10\%}$ hazard levels, respectively. The small difference of collapse ratios implies that different diaphragm designs have small impact on the building performance in terms of collapse. This is because building collapse is more associated with excessive BRB deformation (and fracture) than diaphragm design. Based on the breakdown of collapse ratios, 94% of the building collapses have story drift limit exceeded with large BRB deformation and potential BRB fracture, while only 54% of the building collapses have diaphragm shear angle exceeded.

3) R_s = 1.0 design can be less conservative. From Figure 33 and Table 15, it is shown that for the 1-story building with concrete on steel deck roof under $ACMR_{10\%}$-level ground motions and the 12-story building subjected to MCE-level ground motions, the collapse ratios for buildings with Traditional / Alternative 2 diaphragm design are smaller than those for buildings with Alternative 1 diaphragm design. This is likely because the Alternative 1 design produces stronger and stiffer diaphragms, which forces more inelasticity to occur in the BRB's under the specific scales of ground motions, resulting in larger story drift and more building collapses.

4) Examining Table 15 shows that strengthening the diaphragm produces the most benefit in terms of reducing collapses for the medium height buildings such as 4-story buildings. The 1-story buildings have sufficiently small collapse ratio, and for 8-story and 12-story

buildings, the diaphragm design does not have a huge effect on reducing the number of collapses (average of 1% reduction in collapses). However, for 4-story buildings, strengthening the diaphragm reduced the collapse ratio by an average of 5.3% for the three hazard levels.

5) Based on the evaluation criteria per FEMA P695 methodology, building performance in terms of collapse is considered acceptable if less than 50% of the ground motions at the $ACMR_{10\%}$ level cause building collapse. As shown in Figure 33c, all 1, 4, and 8-story buildings pass the acceptance criteria (with the number of collapses less than 50%), while the collapse ratios for the 12-story buildings exceeds the limit (58.1% for R_s = 2 or 2.5 and 54.5% for R_s = 1). It is also observed under this level of ground motions, the collapse ratios of the buildings with Traditional / Alternative 2 diaphragm design are close to those with Alternative 1 design (2.5% difference on average). Even for the 12-story buildings with collapse ratios slightly larger than 50%, there is only one additional analysis with building collapse for the Traditional / Alternative 2 design compared to the Alternative 1 design, which increases the collapse ratio by 3.6%. This also demonstrates that the collapses of the 12-story building are more associated with the BRBFs and not the diaphragms. Therefore, it is concluded that the alternative diaphragm design procedure with proposed R_s values (R_s = 2 for composite deck diaphragm and R_s = 2.5 for bare deck diaphragm) did not have a significant adverse effect on seismic performance of the archetype buildings compared to R_s = 1.0, and thus these R_s values may be reasonable for use in design of these types of structures.

6) However, the number of collapses for 4, 8, and 12-story buildings associated with DE and MCE hazard levels was larger than expected. The FEMA P695 methodology suggests that the probability of collapse due to MCE ground motions be limited to 10% for each performance group and 20% for individual archetypes. The average collapse ratios for multistory buildings subjected to DE and MCE-ground motions are 6% and 25%, respectively, and the 12-story building has more than 30% of ground motions causing collapse at MCE. These collapse probabilities are larger than those from some other

studies with frame analysis. For example, the probabilities of collapse at MCE in Atlayan and Charney (2014) were below 3.5%. However, in the study by Zaruma and Fahnestock (2018), the results were more comparable, with the numbers of collapses for the baseline prototypes subjected to MCE being 9/44 (20.5%) for 4-story BRBF, 12/44 (27.3%) for 9-story BRBF, and 8/44 (18.2%) for 15-story BRBF. It is hypothesized that the excessive number of collapses at DE and MCE in this study are due to the use of 3D models, and to a lesser extent the consideration of diaphragm deformations. As mentioned in Section 4.3.2.1, median peak resultant story drifts are 50% to 100% larger at the critical first story compared to the story drifts in the x or y direction alone, which significantly exacerbates the P-Δ effect. Also, pushover curves show softening (negative slope) at relatively small roof drift ratio, especially for tall buildings.

7) The performance of archetype buildings investigated in this study in terms of collapse is in general worse compared to results from conventional 2D frame analyses. It can be deduced that the ACMR values for the 1, 4, and 8-story buildings in this study are larger than the acceptable $ACMR_{10\%}$ values equal to 1.96 as given in Table 11, since less than half of the ground motions caused collapse of these buildings, while the ACMR values for the 12-story with collapse probability slightly larger than 50% is slightly smaller than the acceptable $ACMR_{10\%}$ equal to 1.96. In contrast, all archetype BRB frames evaluated in Chen (2010) with number of stories ranging from 2 to 16 passed the evaluation criteria per FEMA P695, with the ACMR values ranging from 2.31 to 4.12. In addition, the case studies in Atlayan and Charney (2014) also showed satisfactory performance of 5-story archetype BRB frames using the ACMR acceptance criteria, where the ACMR values ranged from 2.63 to 3.23. However, in Zaruma and Fahnestock (2018), ACMR values for the baseline prototypes investigated were smaller which were 1.87 for 4-story BRBF (failed), 1.95 for 9-story BRBF (failed), 2.08 for 15-story BRBF (pass). It should be noted that these comparisons may not be ideal because of the different design conditions (e.g., seismic design category) and different criteria for the definition of collapse cases (e.g., story drift limit), etc. Further investigation is desired to examine the 3D effect on the evaluation of seismic performance of buildings.

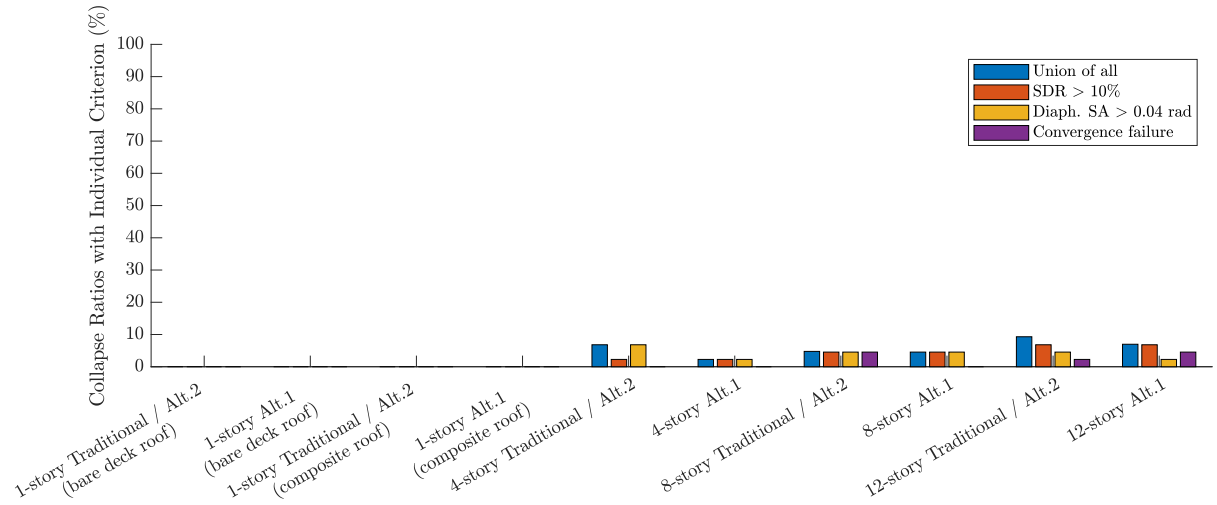

(a) DE

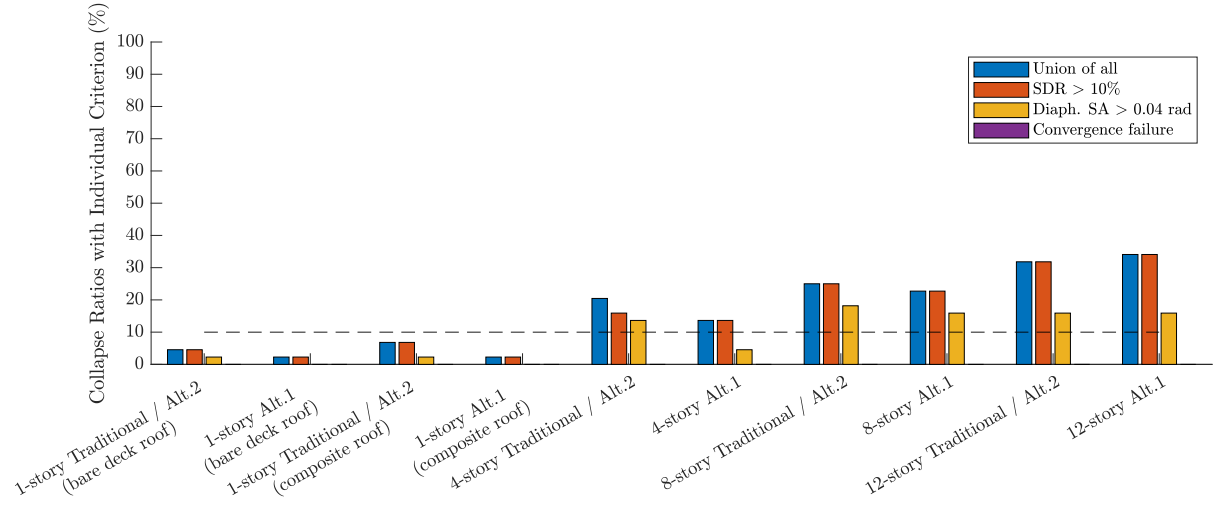

(b) MCE

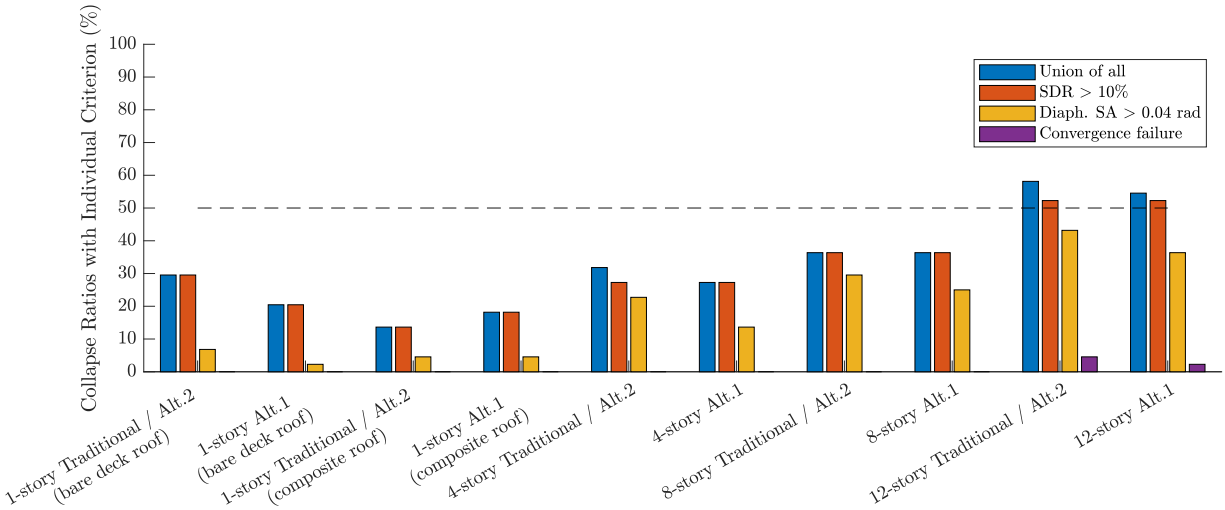

(c) $ACMR_{10\%}$

Figure 33 Collapse ratio breakdown for buildings under three levels of ground motions

Table 15 Collapse ratios for buildings under three levels of ground motions

Archetype Building		DE			MCE			ACMR$_{10\%}$		
		N_{run} [1]	P_c [2] (%)	ΔP_c [3] (%)	N_{run}	P_c (%)	ΔP_c (%)	N_{run}	P_c (%)	ΔP_c [3] (%)
1-story (bare steel deck roof)	Trad. /Alt. 2	44	0.0	0.0	44	4.5	2.3	44	29.5	9.1
	Alt. 1	44	0.0		44	2.3		44	20.5	
1-story (comp. deck roof)	Trad. /Alt. 2	44	0.0	0.0	44	6.8	4.5	44	13.6	-4.5
	Alt. 1	44	0.0		44	2.3		44	18.2	
4-story	Trad. /Alt. 2	44	6.8	4.5	44	20.5	6.8	44	31.8	4.5
	Alt. 1	44	2.3		44	13.6		44	27.3	
8-story	Trad. /Alt. 2	42	4.8	0.2	44	25.0	2.3	44	36.4	0.0
	Alt. 1	44	4.5		44	22.7		44	36.4	
12-story	Trad. /Alt. 2	43	9.3	2.3	44	31.8	-2.3	43	58.1	3.6
	Alt. 1	43	7.0		44	34.1		44	54.5	
Average		44	3.5	1.4	44	16.4	2.7	44	32.6	2.5

[1]: number of runs considered for collapse ratio calculation

[2]: collapse ratio (probability of collapse)

[3]: difference of the collapse ratios between archetype buildings with Traditional / Alternative 2 diaphragm design and archetype buildings with Alternative 1 diaphragm design

5. Conclusions

A series of 1, 4, 8, and 12-story archetype buildings were designed to the current U.S. building code with three different diaphragm designs: a traditional design that uses conventional diaphragm design forces, an alternative design that uses the seismic demand calculated assuming some diaphragm ductility (values proposed for future editions of the building code of R_S = 2 for concrete on steel deck floor diaphragms and 2.5 for bare steel deck roof diaphragms) which ended up the same as the traditional design, and an alternative design with diaphragm demands assuming no diaphragm ductility (R_S = 1.0). Using material models calibrated against test data for diaphragms and BRB, 3D computational models with material and geometric nonlinearity were created. These models were used to conduct modal analyses to study their modal properties, nonlinear pushover analyses to investigate their static behavior, and nonlinear response history analyses to evaluate their seismic performance.

It was found that design office models with a rigid diaphragm assumption can significantly underpredict the natural period (up to 48% underpredicted for some models) and miss some key features of the mode shape. The different diaphragm designs had little effect on the pushover behavior because the pushover analyses used a first mode shape based load pattern and were dominated by BRB inelasticity.

Conversely, response history analyses showed significant inelasticity occurred in the diaphragms as higher modes affected the diaphragm demands. There was also an interaction between diaphragm inelasticity and BRB inelasticity as the two compounded each other to exacerbate the second order effects and cause collapse. Large story drift concentrates at the first story of the building where P-Δ effects are the worst. For the intermediate stories, the peak story drifts are smaller and more uniformly distributed along the building height, while the peak story drifts near the roof become larger due to the "whipping effect" of the building. In addition, because of the 3D effect and diaphragm deformation, the peak resultant story drifts can be twice as large as the story drifts along either orthogonal direction of the buildings. The total story drift considering diaphragm deformation can be significantly larger than the story drift at the BRB frames (up to 80% difference), especially when the diaphragms have smaller in-plane stiffness,

which can result in even larger P-Δ effect. It also indicates that conventional 2D or 3D frame analysis with rigid diaphragm assumption can well underestimate the story drifts of the building.

The diaphragms of the archetype buildings remained almost entirely elastic under DE-level ground motions. The diaphragm shear demands for archetype building with alternative R_s = 1.0 diaphragm design were compared to the elastic diaphragm design shear from ASCE 7 alternative diaphragm design procedure. It was found that ratios of the diaphragm shear demand obtained from the analysis to the design shear given by the alternative diaphragm design procedures in ASCE 7 have an average value of 0.84, indicating a reasonable accurate but slightly conservative prediction of elastic diaphragm shear demand with the design approach.

The performance of the archetype buildings in terms of collapse was evaluated based on the collapse ratio from the results of nonlinear response history analysis. As the number of stories increases, collapse ratio of the archetype buildings tends to become larger. This is more pronounced when comparing the 1-story buildings to other multistory buildings under the DE and MCE-level ground motions, which is contrary to some other studies with 2D frame analysis that have shown low-rise buildings to be more vulnerable. In general, the number of collapses associated with alternative R_s = 1.0 diaphragm design is very close (with an average difference of 2.5% for collapse ratios) to that with traditional or alternative design with R_s = 2.0 for concrete on metal deck diaphragms and 2.5 for bare deck diaphragms, and it is expected that these collapses are more associated with 3D effects than diaphragm design. This is further supported by observing that the difference in median story drifts was negligible between the alternative R_s = 1.0 and alternative R_s = 2.0 or 2.5 diaphragm design. The collapse ratios of all 1, 4, and 8-story buildings with different diaphragm design procedures fall below 50% under the $ACMR_{10\%}$-level of ground motions, so the collapse prevention performance of these buildings can be considered satisfactory based on the evaluation criteria per FEMA P695 methodology. For the 12-story buildings with overall collapse ratio equal to 56% which is slightly larger than 50%, there is only 4% difference between the collapse ratio associated with traditional / alternative R_s = 2.0 or 2.5 diaphragm design and that associated with the alternative R_s = 1.0 design. Therefore, it is concluded that the alternative diaphragm design procedure with proposed R_s values (R_s = 2 for

composite deck diaphragms and R_S = 2.5 for bare deck diaphragms) did not have a significant adverse effect on seismic performance of the considered BRBF buildings compared to R_S = 1.0, and thus these R_S values may be reasonable for use in design of these types of structures.

However, it should also be noted that due to the 3D effect in the analysis with the consideration of diaphragm nonlinearity in this study, there are more collapses than expected for multistory buildings under the DE and MCE-level ground motions, with the average collapse ratios equal to 6% and 25%, respectively. Future study is desired to further understand the behavior of 3D models that consider diaphragm deformations as compared to the more widely used 2D frame analyses, to investigate the 3D effect on the evaluation of seismic performance of buildings, and to define appropriate performance objectives for the evaluation measures such as collapse ratios.

References

ACI. (2014). Building code requirements for structural concrete (*ACI 318-14*) and commentary *(ACI 318R-14)*. American Concrete Institute.

AISC. (2016). Specification for structural steel buildings, (*AISC 360-16*). American Iron and Steel Institute.

AISI. (2016). North American standard for the design of profiled steel diaphragm panels, (*AISI S310-16*). American Iron and Steel Institute.

ASCE. (2016). Minimum design loads for buildings and other structures (ASCE standard). Reston, VA.: American Society of Civil Engineers.

ASTM. (2019). Standard Specification for Carbon Structural Steel, (*ASTM A36 / A36M-19*). ASTM International, West Conshohocken, PA, 2019, www.astm.org

Atlayan, O., & Charney, F. A. (2014). Hybrid buckling-restrained braced frames. *Journal of Constructional Steel Research, 96*, 95-105.

Avellaneda Ramirez, R.E., Easterling, W. S., Schafer, B.W., Hajjar, J.F., & Eatherton, M.R. (2019) Cyclic Testing of Composite Concrete on Steel deck Diaphragms Undergoing Diagonal Tension Cracking. In *The 12th Canadian Conference on Earthquake Engineering, Chateau Frontenac, Quebec, QC.*

Chen, C. H. (2010). *Performance-based seismic demand assessment of concentrically braced steel frame buildings* (Doctoral dissertation, UC Berkeley).

Coffin, L.F. (1954). A study of the effects of the cyclic thermal stresses on a ductile metal. *Translat. ASME*, 76, 931-950.

Eatherton, M.R., Schafer, B.W., Hajjar, J.F., Easterling, W.S., Avellaneda Ramirez, R.E., Wei, G., Foroughi, H., Torabian, S., Fischer, A.W., Briggs, N.E., Madhaven, M.B., Coleman, K. Considering ductility in the design of bare deck and concrete on metal deck diaphragms. In *The 17th World Conference on Earthquake Engineering, Sendai, Japan.*

EERI. (1996). Northridge Earthquake Reconnaissance Report, Vol. 2 Earthquake Spectra - Supplement C to Volume 11 Earthquake Engineering Research Institute.

FEMA. (2009). Quantification of building seismic performance factors, (*FEMA P695*). Applied Technology Council, Federal Emergency Management Agency.

Khorami, M., Khorami, M., Alvansazyazdi, M., Shariati, M., Zandi, Y., Jalali, A., & Tahir, M. M. (2017). Seismic performance evaluation of buckling restrained braced frames (BRBF) using incremental nonlinear dynamic analysis method (IDA). *Earthquakes and Structures, 13*(6), 531-538.

Kircher, C., Deierlein, G., Hooper, J., Krawinkler, H., Mahin, S., Shing, B., & Wallace, J. (2010). *Evaluation of the FEMA P-695 methodology for quantification of building seismic performance factors* (No. Grant/Contract Reports (NISTGCR)-10-917-8).

Luttrell, L., Mattingly, J., Schultz, W., & Sputo, T., (2015). Steel Deck Institute diaphragm design manual - 4th Edition, *(DDM04)*. Glenshaw, Pennsylvania.

Manson, S.S. (1954). Behaviour of Materials under Conditions of Thermal Stress. NACA TN-2933. National Advisory Committee for Aeronautics.

Martin, É. (2002). Inelastic response of steel roof deck diaphragms under simulated dynamically applied seismic loading. Master's thesis, Ecole Polytechnique de Montreal.

Mazzoni, S., McKenna, F., Scott, M. H., & Fenves, G. L. (2006). OpenSees command language manual. Pacific Earthquake Engineering Research (PEER) Center, 264.

Newell J, Uang CM, & Benzoni G. (2006). Subassemblage testing of core brace bucklingrestrained braces (G Series). University of California San Diego. Report no. TR2006/01; 2006

O'Brien, P., Eatherton, M. R., & Easterling, W. S. (2017). Characterizing the load-deformation behavior of steel deck diaphragms using past test data. Cold-Formed Steel Research Consortium Report Series, CFSRC R-2017-02.

Özkılıç, Y. O., Bozkurt, M. B., & Topkaya, C. (2018). Evaluation of seismic response factors for BRBFs using FEMA P695 methodology. *Journal of Constructional Steel Research*, *151*, 41-57.

Rodriguez, M., Restrepo, J., & Blandón, J. (2007). Seismic design forces for rigid floor diaphragms in precast concrete building structures. *Journal of Structural Engineering*, 133(11), pp. 1604–1615.

Torabian, S., Eatherton, M.R., Easterling, W.S., Hajjar, J.F., & Schafer, B.W. (2019). SDII Building Archetype Design v2.0. CFSRC Report R-2019-04, jhir.library.jhu.edu/handle/1774.2/62106.

Veismoradi, S., Amiri, G. G., & Darvishan, E. (2016). Probabilistic seismic assessment of buckling restrained braces and yielding brace systems. *International Journal of Steel Structures, 16*(3), 831-843.

Zaruma, S., & Fahnestock, L. A. (2018). Assessment of design parameters influencing seismic collapse performance of buckling-restrained braced frames. *Soil Dynamics and Earthquake Engineering*, *113*, 35-46.

Appendix

A1. Member Sizes of Archetype Buildings

The sizes of beams, columns, and BRBs of the archetype buildings are given in Table A-1, Table A-2, and Table A-3, respectively.

Table A-1 Beam Sizes of Archetype Buildings

Archetype building	Story	x direction (long direction)			y direction (short direction)		
		Edge beam		Interior beam	Edge beam		Interior beam
		At BRBF	Other		At BRBF	Other	
1-story (bare steel deck roof)	1	W12X16	W12X16	W12X19	W12X26	W12X26	W12X30
1-story (concrete on steel deck roof)	1	W14X26	W14X22	W16X26	W16X36	W16X26	W21X48
4-story	1	W24X62	W16X26	W16X31	W16X67	W16X31	W21X48
	2	W24X62	W16X26	W16X31	W16X57	W16X31	W21X48
	3	W24X62	W16X26	W16X31	W16X40	W16X31	W21X48
	4	W12X16	W12X16	W12X19	W12X22	W12X22	W14X30
8-story	1	W24x84	W16x26	W16x31	W16x100	W16x31	W21x48
	2	W24x84	W16x26	W16x31	W16x100	W16x31	W21x48
	3	W24x84	W16x26	W16x31	W16x100	W16x31	W21x48
	4	W24x84	W16x26	W16x31	W16x100	W16x31	W21x48
	5	W24x84	W16x26	W16x31	W16x100	W16x31	W21x48
	6	W24x76	W16x26	W16x31	W16x89	W16x31	W21x48
	7	W24x76	W16x26	W16x31	W16x89	W16x31	W21x48
	8	W24x76	W16x26	W16x31	W16x77	W16x31	W21x48
12-story	1	W24x84	W16x26	W16x31	W16x100	W16x31	W21x48
	2	W24x84	W16x26	W16x31	W16x100	W16x31	W21x48
	3	W24x84	W16x26	W16x31	W16x100	W16x31	W21x48
	4	W24x84	W16x26	W16x31	W16x100	W16x31	W21x48
	5	W24x84	W16x26	W16x31	W16x100	W16x31	W21x48
	6	W24x76	W16x26	W16x31	W16x89	W16x31	W21x48
	7	W24x76	W16x26	W16x31	W16x89	W16x31	W21x48
	8	W24x76	W16x26	W16x31	W16x77	W16x31	W21x48
	9	W24x62	W16x26	W16x31	W16x67	W16x31	W21x48
	10	W24x62	W16x26	W16x31	W16x57	W16x31	W21x48
	11	W24x62	W16x26	W16x31	W16x40	W16x31	W21x48
	12	W14x30	W14x30	W12x19	W14x26	W14x26	W14x30

Table A-2 Column Sizes of Archetype Buildings

Archetype building	Story	Edge column					Interior column
		At BRBF (x direction)	At BRBF (y direction)		Corner	Other	
			Center	Outer			
1-story (bare steel deck roof)	1	W12X40	W12X40	W12X40	W10X30	W10X30	W10X30
1-story (concrete on steel deck roof)	1	W14X48	W14X48	W14X48	W10X30	W10X30	W10X30
4-story	1-2	W14X109	W14X48	W14X82	W10X33	W10X39	W10X49
	3-4	W14X48	W14X48	W14X48	W10X30	W10X33	W10X30
8-story	1-2	W14x342	W14x82	W14x500	W10x60	W12x87	W12x120
	3-4	W14x283	W14x68	W14x342	W10x49	W10x77	W12x87
	5-6	W14x193	W14x61	W14x257	W10x39	W10x60	W10x77
	7-8	W14x132	W14x48	W14x145	W10x33	W10x49	W10x54
12-story	1-2	W14x342	W14x82	W14x500	W10x60	W12x87	W12x120
	3-4	W14x283	W14x68	W14x342	W10x49	W10x77	W12x87
	5-6	W14x193	W14x61	W14x257	W10x39	W10x60	W10x77
	7-8	W14x132	W14x48	W14x145	W10x33	W10x49	W10x54
	9-10	W14x82	W14x48	W14x82	W10x30	W10x39	W10x45
	11-12	W14x48	W14x48	W14x48	W10x30	W10x33	W10x30

Table A-3 BRB Core Areas (A_{core}), Yield-to-Length Ratios (YLR) and Approximate Stiffness Modification Factors (KF) of Archetype Buildings

Archetype building	Story	x direction (long direction)			y direction (short direction)		
		A_{core} (in^2)	YLR	KF	A_{core} (in^2)	YLR	KF
1-story (bare steel deck roof)	1	1.5	0.85	1.37	1.5	0.77	1.45
1-story (concrete on steel deck roof)	1	3	0.84	1.41	4	0.74	1.54
4-story	1	8	0.86	1.37	10	0.80	1.50
	2	7	0.86	1.37	8	0.79	1.46
	3	5	0.85	1.37	6	0.79	1.46
	4	2	0.85	1.37	3	0.79	1.45
8-story	1	10	0.86	1.37	12	0.76	1.51
	2	10	0.86	1.37	12	0.75	1.53
	3	9	0.86	1.37	12	0.75	1.53
	4	9	0.86	1.37	11	0.75	1.53
	5	7	0.86	1.37	9	0.79	1.46
	6	6	0.86	1.37	7	0.79	1.46
	7	4	0.85	1.37	5	0.77	1.45
	8	2	0.85	1.37	2	0.77	1.45
12-story	1	14	0.71	1.41	16	0.65	1.54
	2	13	0.71	1.41	16	0.65	1.55
	3	13	0.71	1.41	16	0.65	1.55
	4	12	0.71	1.41	15	0.65	1.53
	5	12	0.71	1.41	15	0.65	1.53
	6	11	0.71	1.41	14	0.65	1.53
	7	11	0.71	1.41	13	0.65	1.53
	8	11	0.71	1.41	12	0.65	1.53
	9	9	0.73	1.37	10	0.68	1.46
	10	8	0.73	1.37	8	0.68	1.46
	11	6	0.73	1.37	5	0.69	1.45
	12	2	0.73	1.37	2	0.69	1.45

A2. Modification of Pinching4 Backbone Parameters for Diaphragm Models

The backbone parameters (stresses and strains) of the Pinching4 material model were modified as follows so that the diaphragm shear strength per unit length is consistently represented. The equations used for the modification are derived based on Figure A-1.

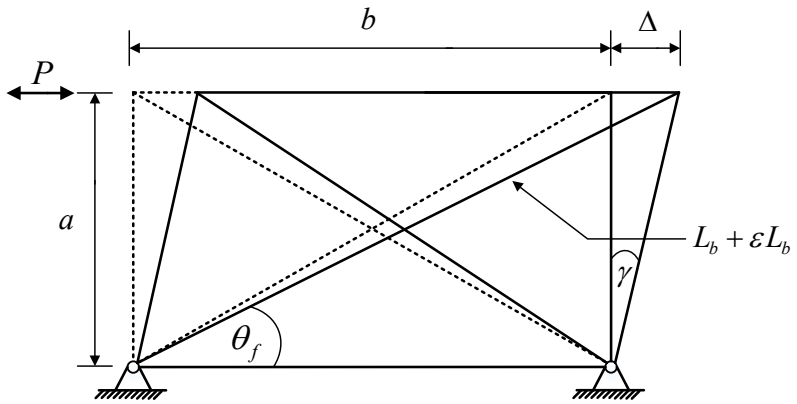

(a) Diaphragm test specimen

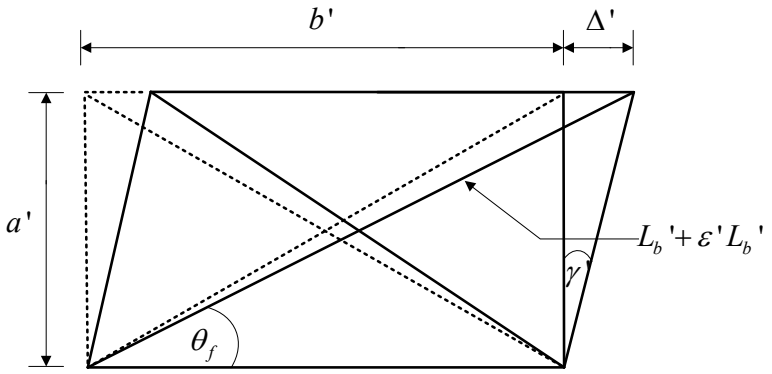

(b) Mesh unit from archetype building models

Figure A-1 Comparison of the diaphragm test specimen and archetype diaphragm mesh unit

1) Stresses

The force in the diagonal trusses, F_b, is given by:

$$F_{bi} = \sigma_i A \tag{A-1}$$

where σ is the stress in the diagonal trusses, A is the area of the diagonal trusses and i is the number ranging from 1 to 4 (corresponding to the Pinching4 stress values).

The relationship between the force, P, and F_b can be established using:

$$\cos\theta = \frac{P_i}{2F_{bi}} \tag{A-2}$$

where θ is the angle in undeformed position (initial angle) which can obtained using:

$$\theta = \tan^{-1}\left(a/b\right) \tag{A-3}$$

where b is the span of the diaphragm specimen and a is the depth of the diaphragm specimen. Substituting Equation A-2 into Equation A-1 yields:

$$P_i = 2\sigma_i A\cos\theta \tag{A-4}$$

The shear strength per unit length of the specimen, S, can be found by dividing Equation A-4 by the span of the diaphragm:

$$S_i = \frac{2}{b}\sigma_i A\cos\theta \tag{A-5}$$

Then the modified stresses for the archetype building models, σ_i', can be obtained using:

$$S_i = \frac{2}{b'}\sigma_i' A'\cos\theta' \tag{A-6}$$

$$\sigma_i' = \frac{b'S_i}{2A'\cos\theta'} \tag{A-7}$$

where b' and A' are the span of each mesh unit and the area of the diagonal trusses in the archetype building models, respectively, and θ' is the initial angle that can be obtained by:

$$\theta' = \tan^{-1}\left(a'/b'\right) \tag{A-8}$$

where a' is the depth of each mesh unit in the archetype building models.

The modified backbone stresses were then scaled by the factors provided in Table 7 and used in the Pinching4 material model of the archetype building models.

2) Strains

The relationship between the diaphragm deflection, Δ, and the strain in the truss member, ε, can be established (based on the deformed geometry) using:

$$\cos\theta_f = \frac{b+\Delta}{L_b + \varepsilon L_b} \tag{A-9}$$

where θ_f is the angle in deformed position (final angle) and L_b is the undeformed length of the truss member which can be obtained using:

$$L_b = \sqrt{b^2 + a^2} \tag{A-10}$$

The diaphragm deflection, Δ, is given by:

$$\Delta = \gamma a \tag{A-11}$$

where γ is the shear angle. Substituting Equation A-11 into Equation A9 yields:

$$\gamma_i = \frac{1}{a}\left[\left(L_b + \varepsilon_i L_b\right)\cos\theta_f - b\right] \tag{A-12}$$

Then the modified strains for the archetype building model, ε_i', can be obtained using:

$$\gamma_i = \frac{1}{a'}\left[\left(L_b' + \varepsilon_i' L_b'\right)\cos\theta_f' - b'\right] \tag{A-13}$$

$$\varepsilon_i' = \frac{1}{L'\cos\theta_f'}\left(\gamma_i a' + b'\right) - 1 \tag{A-14}$$

where L_b' is the undeformed length of the truss member in each mesh unit in the archetype building model and all other terms were defined previously.

Table A-4 provides the values of the Pinching4 material model parameters for the archetype building diaphragm models.

Table A-4 Pinching4 Material Model Parameters Used for Archetype Building Models

Diaphragm	Backbone				Pinching			Strength Degradation					Stiffness Degradation					Energy Dissip.
	ε_1, σ_1 (ksi)	ε_2, σ_2 (ksi)	ε_3, σ_3 (ksi)	ε_4, σ_4 (ksi)	r_{Δ^+}, r_{Δ^-}	r_{F^+}, r_{F^-}	u_{F^+}, u_{F^-}	gF_1	gF_2	gF_3	gF_4	gF_{lim}	gK_1, gD_1	gK_2, gD_2	gK_3, gD_3	gK_4, gD_4	gK_{lim}, gD_{lim}	gE
Bare Deck 1	0.0010, 17.95	0.0022, 23.39	0.0042, 24.84	0.0107, 9.93	0.20, 0.35	0.20, 0.35	0.10, 0.12	0	0.35	0	0.70	0.90	0, 0	0, 0.50	0, 0	0, 0.75	0, 0.90	4.31
Composite 1	0.0005, 82.18	0.0006, 98.94	0.0014, 139.07	0.0134, 62.58	-0.06, -0.06	0.12, 0.12	0.11, 0.11	0	0.83	0.0	0.46	0.33	1.09, 0.14	0.76, 0.47	0.32, 0.12	0.75, 0.10	1.04, 0.61	4.29
Bare Deck 2	0.0010, 28.77	0.0022, 37.48	0.0042, 39.80	0.0107, 15.92	0.20, 0.35	0.20, 0.35	0.10, 0.12	0	0.35	0	0.70	0.90	0, 0	0, 0.50	0, 0	0, 0.75	0, 0.90	4.31
Composite 2	0.0005, 121.00	0.0006, 145.68	0.0014, 204.76	0.0134, 92.14	-0.06, -0.06	0.12, 0.12	0.11, 0.11	0	0.83	0.0	0.46	0.33	1.09, 0.14	0.76, 0.47	0.32, 0.12	0.75, 0.10	1.04, 0.61	4.29

A3. Additional Information about Nonlinear Response History Analysis Results

Table A-5 and Table A-6 provide details for the medians of peak story drifts and diaphragm shear demands of the archetype buildings from the nonlinear response history results.

Table A-5 Medians of Peak Story Drifts at Each Story of Archetype Buildings under Three Ground Motion Levels

Archetype Building	Diaphragm Design	Story	Median of Peak Story Drift at Each Story (%)								
			DE			MCE			$ACMR_{10\%}$		
			x	y	Result.	x	y	Result.	x	y	Result.
1-story (bare steel deck roof)	Alt. 1	1	2.2	2.6	3.2	3.3	3.9	5.3	4.3	4.9	6.6
	Trad./Alt. 2	1	2.1	3.0	3.5	3.4	4.3	5.5	4.5	5.8	7.3
1-story (concrete on steel deck roof)	Alt. 1	1	2.5	2.4	3.1	3.7	3.8	5.1	4.7	4.7	6.6
	Trad./Alt. 2	1	2.5	2.4	3.0	3.9	3.6	5.3	4.6	4.5	6.8
4-story	Alt. 1	1	2.6	2.4	3.2	5.3	3.8	5.7	6.0	4.6	6.9
		2	1.7	1.7	2.1	2.8	2.8	3.9	3.8	3.6	4.6
		3	1.5	1.6	1.8	2.0	2.3	2.7	2.2	2.8	3.1
		4	2.1	2.8	3.0	2.4	3.3	3.5	2.7	3.6	3.8
		whole building	2.7	2.9	3.4	5.3	3.9	5.7	6.0	4.7	6.9
	Trad./Alt. 2	1	2.6	2.3	3.1	5.1	3.9	5.8	6.0	4.8	7.0
		2	1.6	1.6	2.1	2.7	3.0	3.9	3.7	3.7	4.7
		3	1.5	1.7	1.9	2.1	2.5	2.9	2.4	3.0	3.4
		4	2.1	3.3	3.5	2.5	4.2	4.3	2.8	4.5	4.9
		whole building	2.7	3.4	3.7	5.1	4.4	5.8	6.0	5.3	7.0
8-story	Alt. 1	1	2.5	2.4	3.0	3.7	4.0	5.2	5.1	5.0	6.5
		2	1.6	1.8	2.1	2.5	3.0	4.0	3.5	3.9	4.9
		3	1.2	1.1	1.4	2.0	2.0	2.7	2.3	2.5	3.1
		4-6	1.0-1.2	0.9-1.3	1.2-1.5	1.5-1.6	1.3-1.7	1.8-2.0	1.6-1.7	1.6-1.8	2.0-2.1
		7	1.4	1.6	1.8	1.6	1.9	2.1	1.7	2.1	2.3
		8	1.9	2.6	2.8	2.0	2.9	3.1	2.0	3.0	3.2
		whole building	2.5	2.9	3.3	3.7	4.0	5.2	5.1	5.0	6.5
	Trad./Alt. 2	1	2.4	2.6	3.1	3.7	4.2	5.4	4.6	5.3	6.7
		2	1.5	1.8	2.2	2.6	3.0	3.9	3.3	4.1	4.9
		3	1.2	1.1	1.4	2.0	2.2	2.7	2.3	2.7	3.2
		4-6	0.9-1.2	1.0-1.3	1.2-1.5	1.5-1.6	1.4-1.6	1.8-1.8	1.6-1.7	1.7-1.9	2.0-2.2
		7	1.5	1.6	1.9	1.7	2.0	2.3	1.8	2.0	2.4
		8	1.8	2.8	2.9	2.0	3.3	3.4	2.1	3.4	3.4
		whole building	2.5	3.4	3.6	3.7	4.3	5.4	4.6	5.5	6.7
12-story	Alt. 1	1	2.0	2.4	3.0	4.1	4.5	7.0	6.2	6.7	10.2
		2	1.5	2.0	2.4	3.2	3.9	5.5	5.1	5.9	8.6
		3	1.2	1.5	1.9	2.4	3.0	3.8	4.0	3.9	6.2
		4	1.1	1.3	1.5	1.9	2.1	2.7	2.9	2.8	4.0
		5-10	1.2-1.4	1.0-1.5	1.3-1.7	1.4-1.8	1.4-1.8	1.6-2.2	1.6-2.1	1.4-2.2	1.9-2.6
		11	1.4	1.9	2.1	1.6	2.3	2.5	1.7	2.2	2.7
		12	2.2	2.8	3.0	2.3	3.2	3.3	2.3	3.1	3.3
		whole building	2.4	3.3	3.6	4.1	4.5	7.0	6.2	6.7	10.2
	Trad./Alt. 2	1	1.9	2.5	3.0	4.1	4.1	6.0	6.6	5.9	10.6
		2	1.5	2.1	2.4	3.1	3.8	4.9	5.6	4.9	8.8
		3	1.2	1.5	1.8	2.4	2.8	3.6	3.8	3.9	6.1
		4	1.1	1.3	1.5	1.9	2.1	2.7	3.1	2.9	3.6
		5-10	1.1-1.4	1.0-1.4	1.3-1.7	1.4-1.7	1.3-1.7	1.6-2.0	1.5-2.3	1.6-2.2	1.9-2.7
		11	1.4	2.1	2.3	1.6	2.4	2.5	1.7	2.4	2.7
		12	2.3	3.1	3.4	2.4	3.5	3.6	2.4	3.6	3.8
		whole building	2.6	3.5	3.9	4.1	4.7	6.0	6.7	6.0	10.6

Table A-6 Medians of Diaphragm Shear Demands for Archetype Buildings and Comparison to Design Shear

Archetype Building	Diaphragm Design	Story	Median of F_{peak} (kip)									F_{px} (kip)	$\frac{F_{peak}}{F_{px}}$
			DE			MCE			$ACMR_{10\%}$				
			x	y	x or y	x	y	x or y	x	y	x or y		
1-story (bare steel deck roof)	Alt. 1	1	215	291	292	259	357	357	288	401	404.2	419	0.70
	Trad. or Alt. 2	1	240	293	298	299	342	351	336	380	395.2	262	1.14
1-story (concrete on steel deck roof)	Alt. 1	1	367	608	608	442	703	703	470	791	793.2	855	0.71
	Trad. or Alt. 2	1	366	607	607	436	706	706	468	775	783.5	542	1.12
4-story	Alt. 1	1	746	655	816	961	830	994	1031	927	1113	977	0.83
		2	662	773	796	828	929	952	899	989	1025	914	0.87
		3	613	629	727	708	701	818	738	732	840.8	850	0.86
		4	352	441	442	386	480	480	391	504	506.3	419	1.06
	Trad. or Alt. 2	1	757	638	796	958	777	1008	1032	849	1095	524	1.52
		2	626	738	766	782	899	936	878	957	1018	524	1.46
		3	606	645	743	700	736	822	729	765	849.5	524	1.42
		4	384	384	406	431	405	432	443	411	442.7	262	1.55
8-story	Alt. 1	1	740	583	769	1046	810	1092	1175	919	1233	1012	0.76
		2	687	691	820	917	909	1093	1084	1038	1211	980	0.84
		3	656	713	743	844	858	965	937	935	1062	948	0.78
		4	686	563	726	862	659	867	904	676	916.9	916	0.79
		5	616	527	681	725	576	755	778	614	793.8	883	0.77
		6	621	519	624	671	545	702	688	576	704.3	851	0.73
		7	570	512	600	624	547	638	625	550	645.9	839	0.72
		8	331	350	371	346	379	381	351	380	386	419	0.89
	Trad. or Alt. 2	1	738	577	760	1056	749	1084	1220	855	1289	524	1.45
		2	684	706	787	877	869	1048	1062	1007	1198	524	1.50
		3	641	674	741	867	830	956	941	936	1058	524	1.41
		4	681	535	691	811	630	848	883	653	919.6	524	1.32
		5	602	488	623	728	542	734	766	580	781.4	524	1.19
		6	613	493	617	669	532	678	684	546	713.2	524	1.18
		7	548	517	583	620	554	650	630	565	668.7	524	1.11
		8	362	328	373	386	355	396	377	357	396.2	262	1.42
12-story	Alt. 1	1	934	691	965	1259	934	1343	1509	1108	1620	1024	0.94
		2	862	828	984	1124	1194	1329	1431	1326	1688	1003	0.98
		3	827	846	943	1069	1168	1298	1243	1372	1619	981	0.96
		4	790	771	879	963	1017	1100	1064	1076	1256	959	0.92
		5	767	680	810	925	850	954	997	914	1058	938	0.86
		6	729	640	760	883	727	920	936	784	999	916	0.83
		7	691	593	743	826	691	882	870	745	921	895	0.83
		8	750	610	764	848	640	871	882	682	894	873	0.88
		9	654	573	690	734	628	777	764	641	811	851	0.81
		10	644	556	656	758	616	758	756	623	767	839	0.78
		11	652	568	665	729	603	729	729	615	729	839	0.79
		12	412	391	431	436	419	449	435	434	451	419	1.03
	Trad. or Alt. 2	1	943	636	944	1253	839	1256	1570	1014	1669	524	1.80
		2	876	765	937	1113	1049	1243	1422	1275	1607	524	1.79
		3	831	826	949	1046	1091	1228	1268	1391	1524	524	1.81
		4	800	756	868	955	965	1097	1095	1090	1265	524	1.66
		5	774	645	797	908	787	939	1018	887	1086	524	1.52
		6	737	556	739	885	662	897	934	752	963	524	1.41
		7	719	542	751	789	630	837	857	680	915	524	1.43
		8	753	539	753	837	621	837	868	644	873	524	1.44
		9	651	512	670	710	580	753	762	606	771	524	1.28
		10	627	529	635	731	563	735	761	572	763	524	1.21
		11	667	567	685	706	606	710	733	621	742	524	1.31
		12	461	362	461	469	387	469	469	389	469	262	1.76